5-2016

Studying the Conformational Landscape of Biomolecules Using Single Molecule Fluorescence Spectroscopy

Soheila Rezaei Adariani
Clemson University, srezaei@clemson.edu

STUDYING THE CONFORMATIONAL LANDSCAPE OF BIOMOLECULES USING SINGLE MOLECULE FLUORESCENCE SPECTROSCOPY

A Thesis
Presented to
the Graduate School of
Clemson University

In Partial Fulfillment
of the Requirements for the Degree
Master of Science
Physics and Astronomy

---

by
Soheila Rezaei Adariani
May 2016

Accepted by:
Dr. Hugo Sanabria, Committee Chair
Dr. Jousha Alper
Dr. Feng Ding

ABSTRACT

Proteins have many important functions in living system. They are produced from ribosomes as unstructured polypeptide chains of amino acids and then either fold by themselves or with the help of chaperones into their functional, three dimensional structures. However, the details for some proteins conformational changes and how it relates to their function, is still one of the unsolved questions in modern biophysics. Many techniques such as X-ray, NMR and single-molecule Förster Resonance Energy Transfer (smFRET) and multiparameter fluorescence detection techniques can get information about the protein conformational changes, structure, and also dynamic exchange and the equilibrium between different native protein states. Thus, providing insight into how those bio molecular machines really work. The focus of this thesis will therefore deal with: (1) protein structure and conformational changes (2) Fluorescence methods to study the protein conformational changes. (3) *N*-methyl-D-aspartate (NMDA) receptor that is, one member of the ionotropic glutamate receptor family, which requires a co-agonist such as glycine or D-serine for channel activation. Using fluorescence methods we studied the conformational changes of the ligand binding domain of this receptor in the presence of different co-agoinst to understand agonism.

DEDICATION

I dedicate this thesis to my parents. I am deeply indebted to my father's boundless enthusiasm, energy and inspiration and to my mother's magnificent, gorgeous and great kindness.

ACKNOWLEDGMENTS

I am deeply indebted to Dr. Hugo Sanabria for his boundless generosity, encouragement and help. This thesis would not have been completed without his endless support, guidance and enthusiasm for science. Dr. Hugo Sanabria took me under his wing form the start of M.S. and I really was very lucky to benefit from his knowledge and kind manner. He is magnanimous, honorable and great scholar who has helped me to find my way; moreover his special approach to interdisciplinary made to love the field. He welcomed me warmly when I decided to come to the United States of America to work under his supervision.

I am grateful too to Dr. Joshua Alper and Dr. Feng Ding helped me to improve my thesis.

I would like to thank Inna as I learnt a lot from her in the biophysics laboratory.

I would like to thank the rest of staff at Clemson University for helping me in administrative requirement at Clemson University.

I would like to gratitude the financial support of physics faculty at Clemson University.

I would like to thank all the friends I have meet in Clemson University. I am really grateful to group of people in Clemson city who made my time at this city more pleasant and enjoyable.

I thank my family for their endless and immeasurable love and support.

TABLE OF CONTENTS

Page

Table of Contents (Continued)

Page

LIST OF TABLES

LIST OF FIGURES

CHAPTER ONE

PROTEINS

Proteins are one of the vital building blocks of life; they are made of Amino acids. All natural Amino acids have common groups (e.g. the amino group and the carboxyl group), although they have different side chains. Amino acids are bond to each other by peptide bonds to form the polypeptide chain that is the primary structure of proteins.

1.1) Central dogma of molecular biology

Deoxyribonucleic acid (DNA) is a double stranded helix made of nucleic acids that stores and transfers genetic information. Also, it contains the instructions for every protein, and all cell components. Ribonucleic acid (RNA) is a single stranded molecule that exits in different classes; such as ribosomal RNA (rRNA), messenger RNA (mRNA) and transfer RNA (tRNA). It has different funtions such as coding, regulation, and expression. Both RNA and DNA are made of nucleotides which have a sugar called deoxyribose, phosphates and a base such as Adenine (A), Guanine (G), Cytosine (C) and Thymine (T). These nucleotides can interact to each other (e.g. A pair with T and C pair with G). Some differences between DNA and RNA is that in DNA the 2' OH in sugar is removed and it has a double stranded helix, while RNA has 2' OH and it is single stranded. RNA also has the Uridine base instead of Thymine.

The central dogma of molecular biology describes how information from genes transfers to the synthesis of the proteins. This pathway is one direction, from DNA to RNA, and the last step is protein synthesis, and it never goes backwards. This theory was explained by Francis Crick in 1956 (Crick & Watson, 1956), and this process has two main steps:

transcription and translation. Proteins are made based on the information on DNA. The DNA is located only in the nucleus and proteins are made in ribosomes contained in cytoplasm. RNA can be found in nucleus and also in cytoplasm.

Particular segment of DNA is transcribed with the enzyme RNA polymerase. This segment is copied to RNA. After that, RNA can transfer the information to the ribosome, where it puts together amino acids based on that information. This kind of RNA is called messenger RNA (mRNA), but there are other kinds as well. For example, transfer RNA (tRNA) that transfers amino acids to ribosomes. Ribosomal RNA (rRNA) exists in the ribosome. The ribosome matches the sequence information from the mRNA to amino acids. It reads three bases at a time; these bases are also known as a codon. These codons are matched to the tRNA that has the three complementary bases in its anticodon part. Bases are paired via the important rule: C bind to G and A binds to U. So, the ribosome moves along mRNA and matches three bases, and adds one amino acid to the polypeptide chain to make a protein. At the end, when the ribosome reaches the stop codon, it can release the polypeptide chain and mRNA. The protein will fold to its native structure (Alberts et al., 2014). Therefore, the central dogma theory is helpful to know how proteins are made of. Moreover, if something happens in this pathway (e.g. mutation in DNA structure), then the protein cannot be synthesized correctly and consequently it cannot have its proper function and structure. For example, NMDA receptor that is one of the vital receptor in membrane, if it has mutation then the passing the ions through cell will be disturbed and it can create many disease.

1.2) Classification of amino acids

Amino acids can be categorized in different ways, but one of the common ways to classify them is based on their polarity. There are 20 common proteinogenic α-amino acids in eukaryotes, which can be categorized in 4 major groups (Figure 1.1) (Nelson, Lehninger, & Cox, 2008).

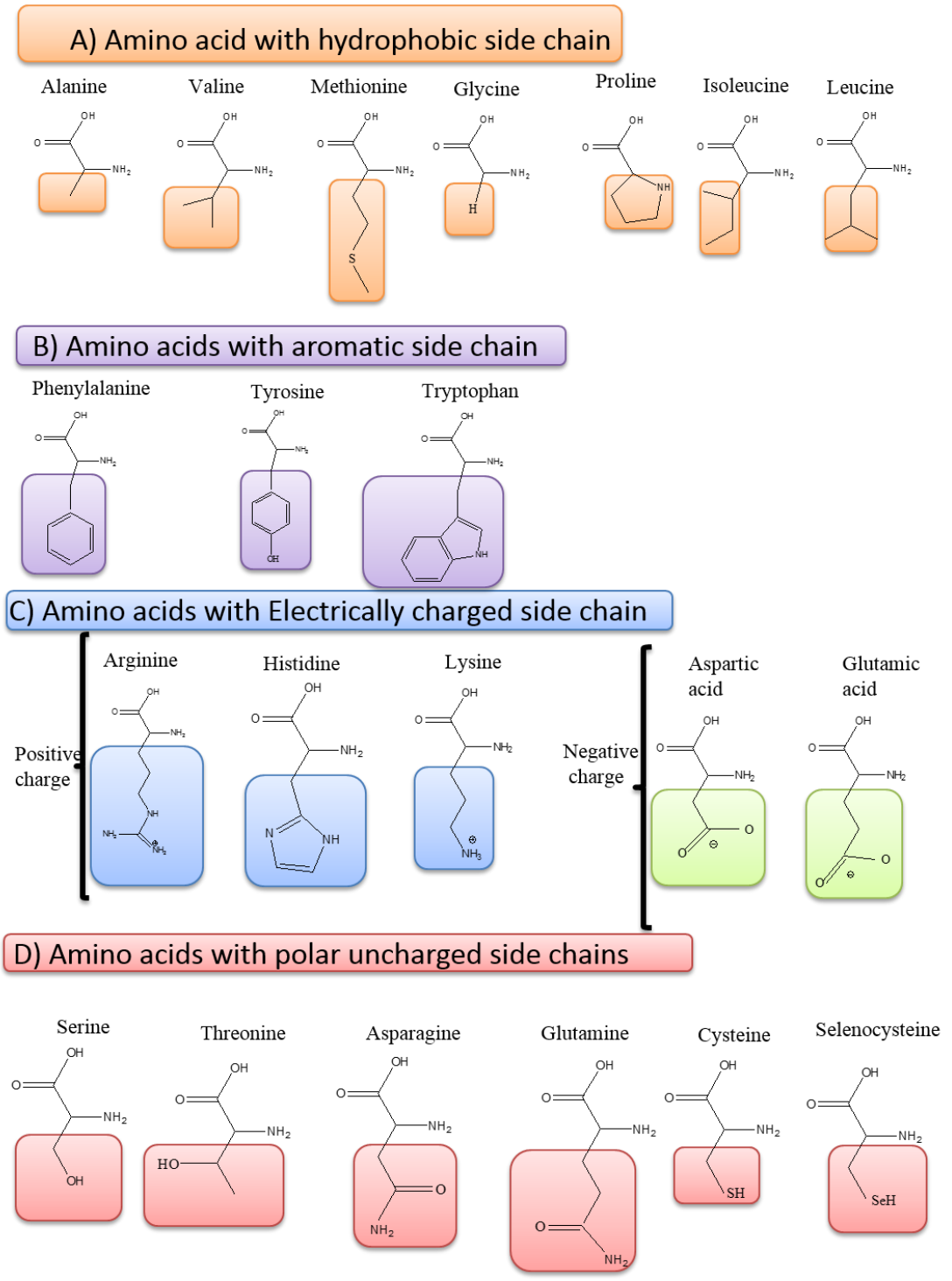

Figure 1.1 Structures of amino acids. There are 20 Proteinogenic α –amino acids in the eukaryotes in four major groups based on their side chains.

Amino acids with hydrophobic side chains that have low contact with water include Alanine, Valine, Leucine, Isoleucine, Glycine, Methionine, and Proline. Because these have hydrophobic components, most of the time these amino acids are in the core of the proteins and they can help that protein fold in the correct conformation. The hydrophobic interaction is vital in stabilizing protein structure. For soluble domains non-polar amino acids tend to avoid contact with water and they reduce the energy of the system by getting close to each other; consequently, the polypeptide chain collapses. The hydrophobic side chains make up the protein core and the hydrophilic residue tends to stay on the outer edge. Hydrogen bonds at the shell help to isolate the hydrophobic core. These amino acids can also be located on the surface for protein-protein interaction.

Amino acids with Aromatic side chain include Phenylalanine, Tyrosine and Tryptophan. They are approximately nonpolar and can have hydrophobic interactions. They can also absorb light at 280 nm. This is useful for studying the protein structure (Groves, 2005). However, these amino acids are rare in proteins. For example, tryptophan can be found more than the two others, and is about 1 mole % in proteins. The tryptophan in proteins have higher sensitivity to local environments compare to Tyrosine and Phenylalanine. For example, collision quenching mostly because of presence of lysine and histidine near indole group, conformational transition, denaturation and binding that can affect environment of indole group in this amino acids. Moreover, protein fluorescence that has more than one of these amino acids is more complex, because the local environment can affect the emission of each.

In some proteins that do not have tryptophan, it can be inserted into the protein to study the protein folding and dynamics. By studying proteins that have one tryptophan, scientists have been able to obtain information about the effects of local environments in the proteins. Studies of single-tryptophan proteins can be useful for investigating protein folding, dynamics and function (Lakowicz, 1999).

Amino acids with electrically charged side chains are aliphatic, and they have either positive or negative charge. They are usually located on the surface of the protein, and can interact via hydrogen bonds with water, other polar groups, or the active site. Their role is to stabilize the protein. The positively charged amino acids are Lysine, Arginine, and Histidine. Lysine has a positive ε-amino group (pKa=11), Arginine has a positive guanidinium group (pKa=13), and Histidine has a positive imidazole group (pKa=6). Two amino acids with negatively charged are Aspartate and Glutamate, that both have carboxyl group with negative charges in their side chain in pH=7.

Amino acids with polar uncharged side chains can interact more with water, because of the hydrogen bond between them and water. They include Serine, Threonine, Cysteine, Selenocysteine, Asparagine, and Glutamine. The Serine and Threonine have hydroxyl groups, and Cysteine has a sulfhydryl group, and Asparagine and Glutamine interact via amide groups. Since these amino acids are neutral sometimes they are found in the active sites of enzymes and the catalytic sites of proteins. Also, some of these amino acids - such as serine, threonine and asparagine - are important in forming glycoproteins and sites for linkage of sugars to proteins. Moreover, serine and threonine are involved in reversible phosphorylation for regulation of energy metabolism in the human body.

The variant in amino acids helps that protein have flexibility movement and they can fold in their native three dimension structure by having interaction between different amino acids in diverse part of the proteins such as proteins in membrane and receptors for example NMDA receptor that the sequence of amino acids on that are necessary to interact with membrane that has hydrophobic and hydrophilic feature. Also, there are some amino acids such as Glycine, L-Alanine and D-Serine that they can bind to as regulator to some proteins like NMDA receptor.

1.3) Protein structure

The sequence of the amino acids can form polypeptides and biopolymers and it is called protein formation. There are four different structures. All proteins have the first three structures, and some special proteins also have a fourth structure (Figure 1.2).

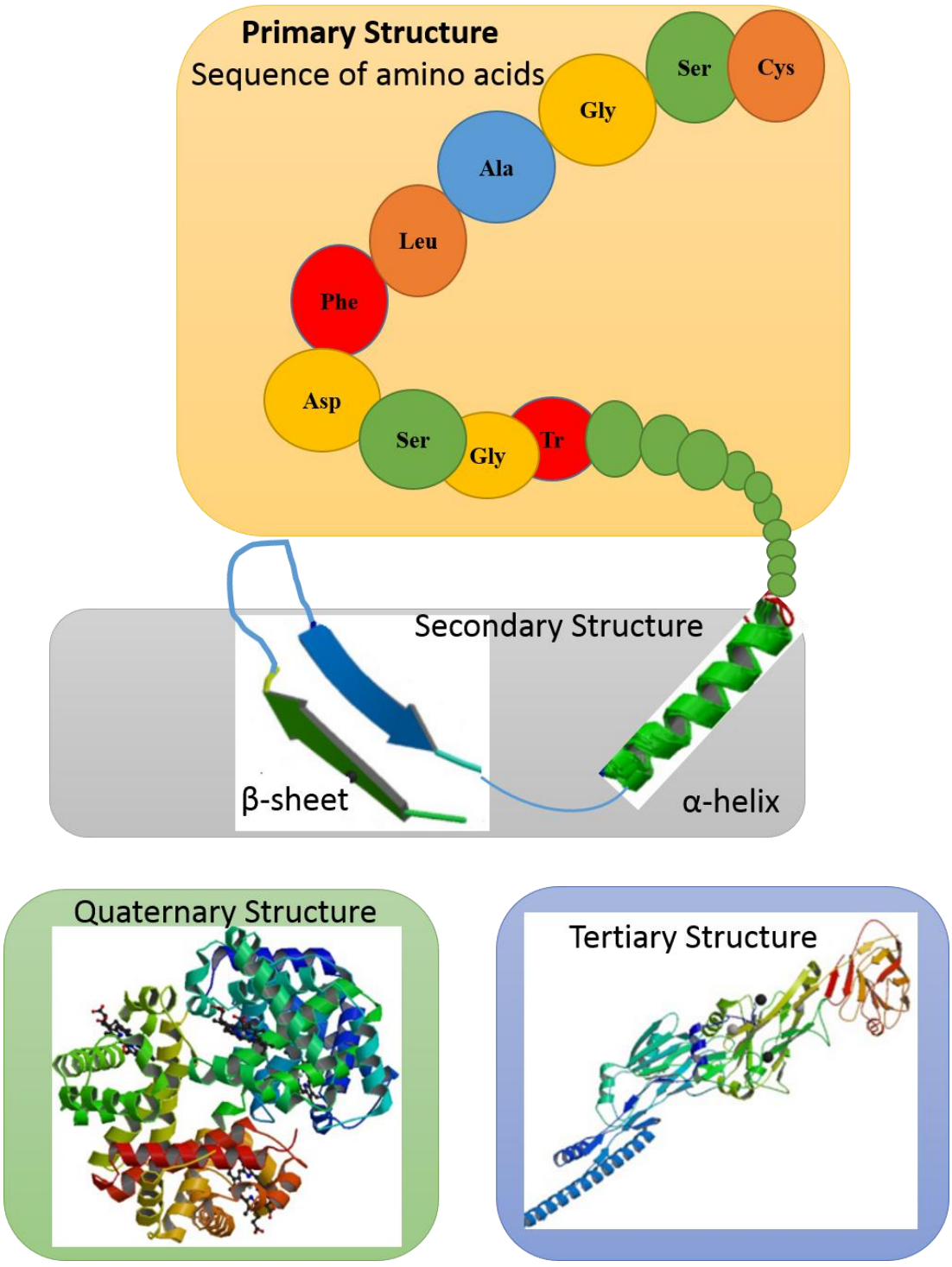

Figure 1.2 Protein structure from primary structure to quaternary structure. Primary structure is sequence of amino acids, however in secondary structure the local interaction between amino acids lead to create α-helix (PDBID:2MJ2). and β- sheet PDBID: 3NI3), moreover on tertiary structure PDBID: 4TSH) protein fold and has function and in quaternary structure PDBID: 3WTG) some proteins can interact with each other (modify from Wikipedia: https://en.wikipedia.org/wiki/Protein_structure).

In the primary structure of the proteins, amino acids are connected to each other by peptide bonds. Therefore, the sequences of amino acids create the primary structure of the proteins. When two amino acids connect via peptide bonds, a water molecule is released because of the interaction between carboxyl group of one amino acid with the amino group of the other. The amino group in one end of the polypeptide is known as N-terminus and the carboxyl group on the other end is known as C-terminus.

There can be a resonance between the carboxyl group and the Amide group due to the double bond in peptide bonds, and all six atoms that are involved in peptide bonding can be in the planar configuration. The angles that are involved in peptide bonds are known as Ψ (psi) for Cα- C bond and Φ (phi) for N-Cα. These two angles can rotate from 0˚ to 180˚, but they cannot have all of the values between 0˚ to 180˚. Some, like Φ =0˚ and Ψ=0˚, are not possible because of interaction between the atoms in the bond. All allowed values for these two angles are plotted in the Ramachandran plot (Richardson, 1981). This plot can also show the prohibited conformations and angles for Ψ and Φ. More than 77% of the conformations are not possible for proteins. Therefore, the Ramachandran plot is useful to get information about all possible values for conformation and angles of proteins.

The secondary structure describes the local interaction between different part of the proteins via hydrogen bonds between the carboxyl group of one amino acid and the amide group in another. Two common secondary structures are the α-helix and the β-sheet.

In an α-helix, amino acids interact with each other by hydrogen bonds to form twisted polypeptides chains which arrange in a spiral shape. In this conformation, the amino acids are ordered along the imaginary axis and the side chains are toward the outside of the helix. The extension of each turn is about 5.4 A˚ and Φ=-60˚ and Ψ=-45˚ to -50˚. In α-helix, first and fourth amino acids in the turn have internal hydrogen bonds between the oxygen of the carboxyl group and the hydrogen of amide group. This pattern is repeated along the helix except at both ends.

For the β-sheet, the amino acids bond alongside each other via hydrogen bonds and create a zigzag conformation of polypeptide chains. The side chains orient towards the outside again, but each side chain points in the opposite direction from the last. The β-sheet polypeptide can be arranged in parallel, which has the amino to carboxyl orientation or antiparallel, which has the opposite amino to carboxyl arrangement. Therefore, they have different hydrogen patterns, with antiparallel having a longer repetition period (7 A˚ for antiparallel and 6.5 A˚ for parallel). Also, the α-helix and β-sheet are connected via turning or looping regions together.

Additionally, a polypeptide chain of amino acids can interact via nonlocal interactions. Amino acids in different parts of the polypeptide chain can influence each other, and as proteins can fold in three dimensions. In other words, the tertiary structure results from long range interaction (e.g. non-covalent bonds and sulfate bonds across polypeptide chains) between side chains. This interaction is usually stronger than hydrogen bonds. Moreover, amino acids with hydrophobic side chain usually are in the core, and the aliphatic amino acids are around to create stable fold structure for proteins. Some proteins

like PSD-95, ASAP1 have a super-tertiary structure that is different from a normal tertiary structure. It refers to a structure that has multiplicity states because of the dynamicity of the protein domains, but the tertiary structure has one state, (Varadi, Vranken, Guharoy, & Tompa, 2015). Based on the protein structure, the function of the protein can be different. For example, some proteins such as α-Keratin have α-helixes and they coil together. So, this protein is very strong and can be found in hair, and nails. Collagen is very similar to α-Keratin; it has high strength and it is found in connective tissue. It also has α-helixes, but the helix is left handed in this protein and it has three amino acids in each turn. So, the protein structure is very vital in determining the function of them.

Quaternary structure is created in larger protein complexes via hydrophobic interactions between side changes of the amino acids. This is the arrangement of a number of folded proteins subunits into larger structures (Brändén & Tooze, 1999). Therefore, the orientation and the angles between amino acids in their structure are key factors to determine their conformational changes and structure of the proteins, for example NMDA receptor, and also the function is related to the structure of the proteins.

1.4) Energy landscape

One of the common models for the energy landscape of protein folding is described by the folding funnel. In 1986, Levinthal explained that each protein has a large number of degrees of freedom, and by calculating the all possible energies, he obtained the astronomical number for all conformation of the protein (Bryngelson, Onuchic, Socci, &

Wolynes, 1995; Deniz, Mukhopadhyay, & Lemke, 2008). He noted that in protein folding, a molecule does not go through all possible energy pathways, because if this happened, it would take a very long time for the protein to fold in its natural conformation. This was named the Levinthal paradox (Zwanzig, Szabo, & Bagchi, 1992). So, the folding pathway depends on the free energy landscape can describe by folding funnel. It starts in a flat area where the protein has multiple conformational changes between folded to unfolded states and reverse. Between folded to unfolded state, they are intermediates and molten globular structure. At the end of the funnel is the folded protein conformation that has the minimum free energy (Figure 1.3) (Bryngelson et al., 1995; Hartl, Bracher, & Hayer-Hartl, 2011).

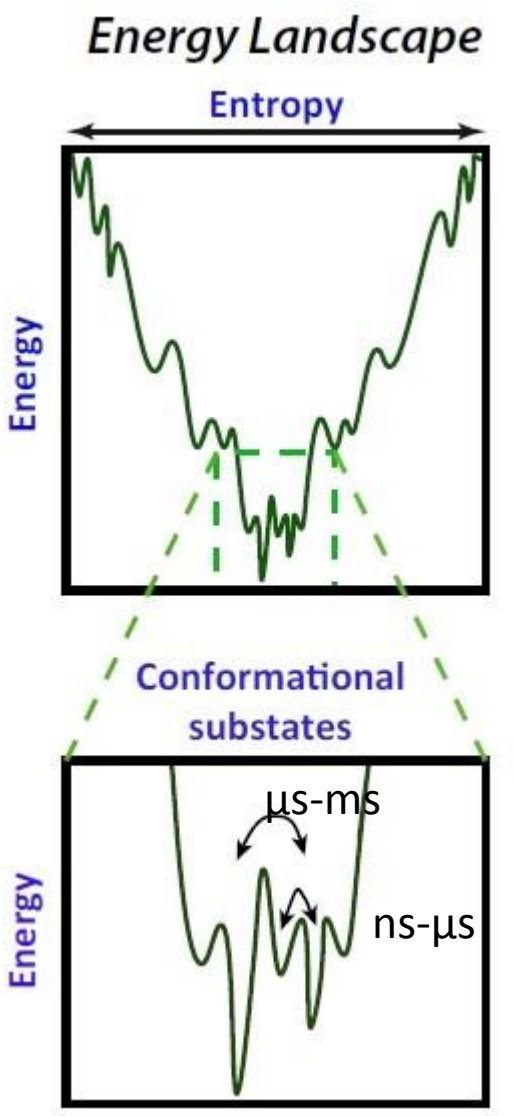

Figure 1.3 Protein folding funnel. IT describe protein folding pattern, since each protein has different conformational changes and protein fold in native state that has minimum free energy.

1.5) Methods to probe protein structure

Protein folding and conformational changes in native states can be studied by various methods. Some of important methods are describe below (Heilemann, Hwang, Lymperopoulos, & Kapanidis, 2009). We want to know, how multiple conformations are

important on the function of proteins. For that, we want to obtain as many as conformations as possible and link them to their function of NMDA receptor. Studying protein function is very important because it leads to knowledge about how proteins work (Skoog & Leary, 1992).

X-ray crystallography: This method is useful for identifying the structure of molecules or atoms in a crystal. Those x-rays beams that are scattered by the electrons of the atoms in the crystal. When an x-ray collides with atoms, it can be diffracted. The amplitude of x-ray diffraction increases with an increase in the number of electrons. The waves of diffraction can interact with each other, and this interaction can be in the same phase or a different phase. The x-ray diffraction patterns of single molecules are weak and extremely difficult to detect, but in crystals, the larger number of molecules are arranged in the same orientation. Thus, the crystal acts as an amplifier. Therefore, by using the diffraction patterns of the atoms in crystal and Bragg's law, which links the wavelength of electromagnetic radiation to the diffraction angle and the lattice spacing in a crystalline sample, it is possible to determine the position of the atoms in the crystal and make a three dimensional map of the molecule. Then, from these patterns, it is possible to use mathematical methods, for example Fourier transform, to calculate the electron density of the crystal (Powell, 1999). Although, some proteins such as membrane proteins are difficult to be crystallized (Smyth & Martin, 2000). Also, there are two major problems in X-ray crystallography, creating large and huge quality crystal is hard and also there is the phase problem that is refers to losing information when we make physical measurement. However, by using some methods such as the molecular replacement

(MR), multiple isomorphous replacements (MIR) and multiple wavelength anomalous dispersion (MAD) it is possible to fix this issue.

Nuclear magnetic resonance (NMR): Placing the molecules in the powerful magnetic field can induce a resonance in their nuclei, and then, by NMR, it is possible to measure the chemical shifts of the atoms from the resonant frequency of a nucleus relative to a standard (e.g. Tetramethylsilane *TMS*) in a magnetic field. This chemical shift depends on their distance from each other and the group next to them based on organic group. Indeed, in NMR unlike infrared or uv-visible spectroscopy, the signal depends on external magnetic field and frequency. Since the magnetic field will be different from each other. Consequently, the resonance frequency will be diverse. But, by using the reference the location of the NMR signal in a spectrum can be compare together. The reference usually added to the sample. Thus, the reference should be reactive, remove easily, and has sharp signal that does not interfere with the signal of the sample for example TMS (Jacobsen, 2007). In NMR, the nuclei of the samples can absorb the magnetic field. Since the nucleus of each atom has spin, in the present of the external magnetic field, the energy level of the atoms will split. This splitting depends on the number of the protons and neutrons. The spin of the nucleus is different, for example, when the number of protons plus the number of neutrons is odd then the nucleus has half-integer spin.

Without the external magnetic field, the energy level is the same and cannot be split. So, each level has a magnetic quantum number. The re-emission of the electromagnetic and magnetic field, and also the magnetic field of the atoms, can give information about the

position of the atoms and the structure. Furthermore, it is possible to obtain possible structures for the protein, although the lack of sufficient restraints is one of the problems in this method (Cavalli, Salvatella, Dobson, & Vendruscolo, 2007). Although, one dimensions NMR, it has one dimension frequency and the chemical shift depends on chemical environment such as the number of the nuclei sites. But, it does not give any information about the mechanism to get information about the structure of the molecules. However, there are other methods in NMR such as two dimensional NMR that has two frequency dimensions and in general it can give information about the interaction between two nuclei. Then, by using Fourier transformation the two dimensional spectrum can be converted to three dimensional contour maps, and can give information about protein structures and dynamic (Bax, 1989).

Circular dichroism (CD): Circular dichroism (CD) reports on the differences in absorption of left and right circularly polarized light. However, the molecule must be chiral (optically active). Positive CD refers to when left circularly polarized light absorbs more than right, and negative CD means when right absorbs more than left. When left and right are similar, there is no signal (Fasman, 1996). So, this is useful to get information about secondary structure such as α-helix and β-sheet conformations in the protein. For example, when there is band at 222 (nm), it points to an α-helix, and 216 (nm) and 218 (nm) indicates the β-sheet. Since they are chiral, their secondary structure is different. In protein folding pathways, the secondary structure of the protein will be changed. Sometimes when the protein unfolds, the α-helix is changed to misfolding and

then creates a β-sheet. Therefore, by using CD, it is possible to study folding and unfolding pathway through changes in secondary structure (Greenfield, 2006).

Fluorescence: Fluorescence spectroscopy is a powerful method to study the protein structure, dynamics, and interaction, and protein conformation (Olofsson & Margeat, 2013). Some proteins have aromatic amino acids that have fluorescence absorption and emission. It is possible to study the proteins by fluorescence spectroscopy in different time scales (from picoseconds to seconds) by site-specific labeling (Lakowicz, 1999). It is described in chapter two in more details.

For studying the ligand binding domain of NMDA receptor, previously x-ray crystallography was used. Their results did not show different between partial agonist and full agonist. In this thesis, we used Fluorescence methods and it shows at least three conformational changes and the results are explained in chapter three.

1.6) Protein dynamics

Biological systems have dynamic behaviors across very broad time scales, from very fast (on the order of 10^{-12} second) covalent bond vibration, to slow movement (on the order of 10^{18} second) for diversification of humans (Phillips, Kondev, Theriot, & Garcia, 2012). In Figure 1.4, it shows several different proceses at various time scales. For example, enzymes are active from the milliseconds to seconds time scale; since they want to catalyze the reaction, they should react fast. Enzymes carry out nearly all the thousands of chemical reactions taking place in a cell. So, their dynamics are related to their function. Fully folded proteins are inherently dynamic on a wide range of time scales – starting from bond vibrations in the fs range, to side chain rotamers in the ns range, up to

larger domain motions in the ms range – and fulfill a broad variety of important functions inside and outside the cells. Additional proteins are needed to provide the cell's structure (cytoskeleton), to transport ions and small molecules, and to protect against foreign particles, bacteria and viruses. These mediated functions generally occur on time scales larger than ms. By using methods listed below, it is possible to study processes in different time scales. By using direct observation methods, we can watch the subjects without altering the environment. The processes that include the majority of the steps in the cell cycle which are a type of individual transformation process occur between milliseconds to hours can be studied. For longer processes, from microseconds to years, the fixed time points method is useful to study the population changes. For example, the bacterial growth curve, which is the kinetic curve that represents the cell divisions by the bacterial population, grows. For continuous processes, such as axonal transport that takes from minutes to days, the pulse-chase method where the label component will be studied through the metabolism or transporting processes is more useful. For understanding protein function, it is vital to know about the structure and their dynamic motion (Phillips et al., 2012).

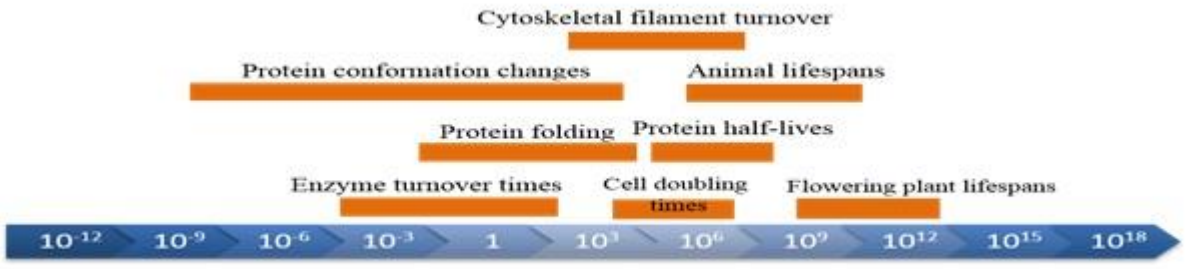

Figure 1.4 Biological time scale. Biological systems have dynamic motion over very broad time scales, that each one based on their structure and function work in specific time scales.

1.7) Bimolecular function

As is mentioned previously, proteins have a sequence of amino acids and they can fold in a three dimensional structure. However, they are not rigid and they have dynamic motion, so they can have different functions in a living cell. All proteins, to some extent, bind or interact with other proteins: for example, actin filaments are the combination of the actin molecules that are bound to each other. A protein that binds to another protein is known as a ligand. There are three common model to explain ligand binding, those are include lock and key, induce fit and conformational changes. In lock and key model, the ligand fits exactly to the binding site like a key that can fit to a specific lock. Another model is induced fit where the substrate binds to active site on the enzyme weakly and then the substrate can induce the conformational change, so they will bind together. In the conformational selection model, all the conformation exit in equilibrium, but by binding the ligand the equilibrium will shift and the proper conformation is favored. If small changes occur - even in parts of the protein that do not have contact with ligand - then the protein structure can change and the function will be altered.

There are various types of proteins; some proteins interact with the surface while others can act as an enzyme to catalyze a reaction. For example, receptor are the proteins that can receive chemical signal, and usually specific ligands can bind to become active and biochemical events can occur as a result. For example, NMDA receptor needs glycine and glutamate at the same time to become active. The NMDA is a heteromeric non-selective cation channel.

Antibodies are produced by the immune system to interact with foreign molecules and to bind specifically to the antigen. Usually, each antibody has two binding sites in its surface and they have several loops of polypeptide chain held together by disulfide bonds inside each loop. If the length and sequence of amino acids in the loop change, then the antibody will interact with another antigen, and the function will be completely changed. Another type of protein that is very vital for cells, are enzymes that can make or break covalent bonds in the cell and catalyze chemical reactions; they do not change during the reaction, but simply speed up the reaction. Each enzyme can specifically catalyze a reaction - for example, proteases that, by hydrolyzing the amino acids, can break down the proteins. Therefore, the chemical properties can affect the protein function (Phillips et al., 2012).

1.8) Summery

Proteins are synthetized by ribosomes. For producing the protein the information in the DNA is transferred by the RNA (the process is described by central dogma of molecular biology). Proteins are made of amino acids that are fold to tertiary structure. Based on their structure, they have specific function. Since there is not a comprehensive method that could get all information about the protein conformation changes.

I used, different fluorescent methods (chapter two) to understand protein conformational changes and their function. Our goal is to study the conformational changes of ligand binding domain of NMDA receptor, in the present of different ligands that lead the receptor to be activated.

CHAPTER TWO

FLUORESCENCE

Bu using fluorescence methods such as Förster resonance energy transfer (FRET), it is possible to measure rigid and dynamic of biomolecules. Using fluorescence, we can measure very broad time scale (from ps-s). In this chapter this topic is explained in more details.

2.1) Principle of fluorescence

At room temperature, majority of the electrons in molecule occupy the ground state (S_0), by absorbing the photons the electrons (around 10^{-15} second) can be excited from ground state to excited states (S_1-S_n). Within 10^{-13} to 10^{-11} seconds they can come back to S_1, but the relaxation from S_1 to S_0 is around 1000 time slower, and this emission is known as luminescence.

Luminescence is divided in two categories: fluorescence and phosphorescence. In phosphorescence the molecule first undergoes a transfer from the singlet to the triplet state T_1 (intersystem crossing). For the photon to be emitted, the system has to return to the singlet state (forbidden spin reversion). The triplet state is thus a long living state and the emission of phosphorescence can take up to several minutes. In fluorescence, the electron relaxes directly from excited state (S_1) to ground state (S_0), so it is faster compared to phosphorescence (in order of nanosecond). However, the emission process is red shifted compared to the excitation process, because it has lower energy (Ahmed et al., 2013).The excitation and emission process can be summarized through a Jablonski diagram (Figure 2.1 A).

Fluorophores are the molecules that emit fluorescence. Fluorophores can be categorized in two groups: extrinsic fluorophores such as Alexa 488, and intrinsic fluorophores like green fluorophores protein (GFP). As it shows in figure 2.1B, intrinsic fluorophores like GFP proteins are usually inserted in in the N-terminal or C-terminal of another proteins. However, the extrinsic fluorophores are smaller and can be inserted in specific positions in the biological system, without interrupting the protein sequence (Lakowicz, 1999).

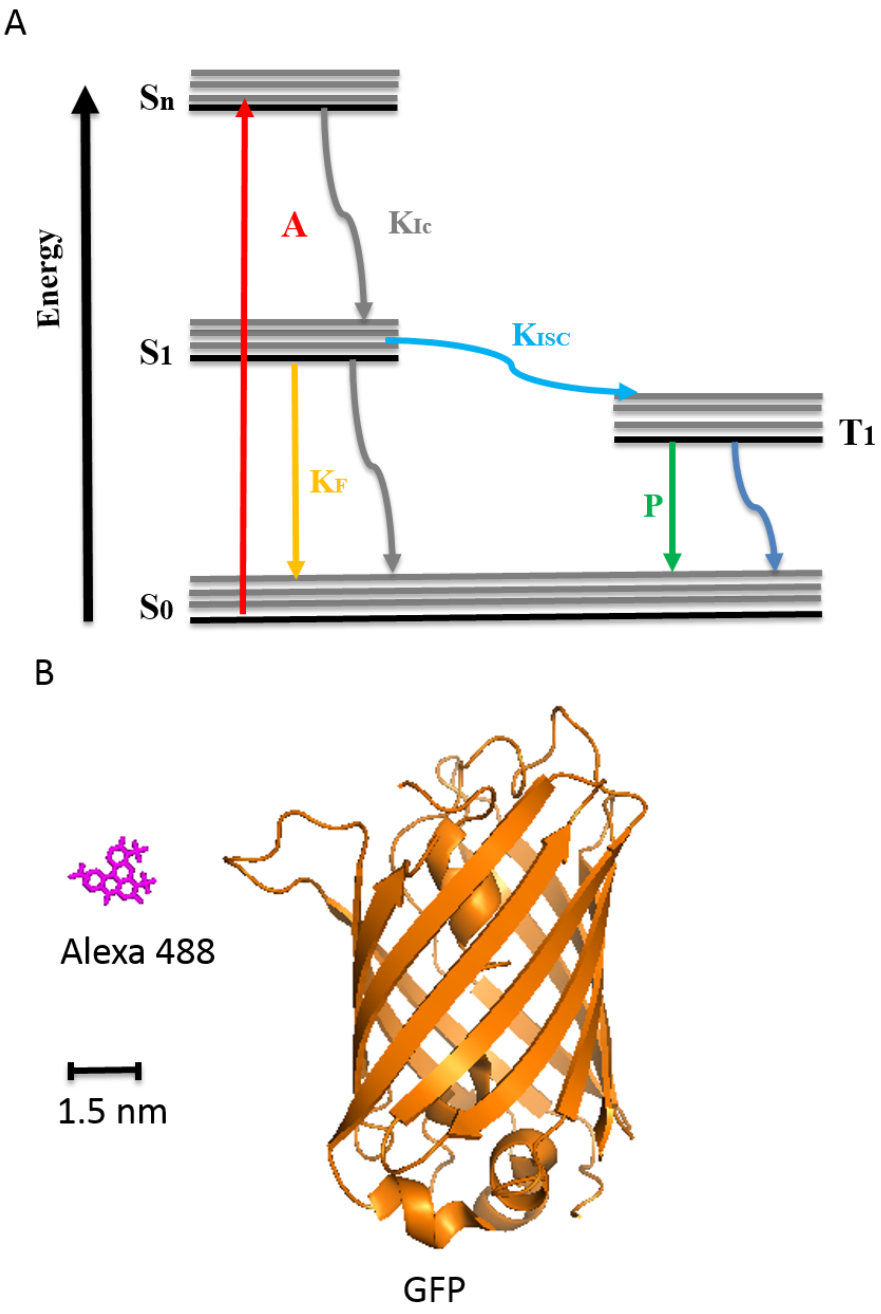

Figure 2.1 Jablonski diagram. The fluorophore after absorbing the photon (A, red) from group state (S_0) will be excited to excited state (S_1-S_n), and then the emission can be occur in different ways, fluorescence (KF, orange), phosphoresce (P, green) and internal relaxation (KIC, gray) B)structure of Alexa 488 and GFP (PDBID:4ZF3).

2.2) Fluorescence lifetime

The average time that the electrons spends in the excited state before coming back to the ground state follows the first order equation:

$$\frac{dN}{dt} = -k_f N \quad \text{Eq. 1}$$

That N is the number of molecules in S_1 and k_f is the rate constant for the emission of fluorescence (Figure 1.5). The solution for Eq. 1 leads to an exponential decay that describes the fluorescence lifetime (Sun, Rombola, Jyothikumar, & Periasamy, 2013). It is a fast process, usually in order of nanosecond to picosecond. This fluorescence emission is described by an exponential decay *f(t)* that depends on *N* and quantum yield ϕ_f (it describes later in this chapter in more details), and the fluorescence lifetime τ is the inverse of the characteristic decay rate constant k_f which is the emission of fluorescence (Engelborghs & Visser, 2013). Moreover, fluorescence lifetime τ refers to the lifetime where the initial maximal intensity after excitation *f(0)* dropped to 1/*e* of its original value:

$$f(t) = f(0)\exp(-t \cdot \mathrm{k_f}) = F(0)\exp(-t/\tau) \quad \text{and} \quad f(t) = \phi_f N \qquad \text{Eq. 2}$$

the fluorescence lifetime depends on various factors, for example viscosity of the solvent, and sometimes the local enviroment can quench fluorescence to shorter lifetime. Because the environment of the fluorophore can be heterogeneous and the lifetime cannot be longer modeled as a mono exponential decay and therefore a multi exponential model should be used:

$$f(t) = \sum_i x_i \exp(-t/\tau_i) \qquad \text{Eq. 3}$$

where τ_i are the fluorescence lifetimes of each decay process (quenched or non-quenched) and x_i is the respective fractions.

Two averages could be calculated. The species average life time and the average fluorescence lifetime.

$$\langle \tau \rangle_x = \sum_i x_i \cdot \tau_i \qquad \text{and} \qquad \langle \tau \rangle_f = \frac{1}{\langle \tau \rangle_x} \sum_i x_i \cdot \tau_i^2 \quad \text{Eq. 4}$$

Another fluorescence quantity that is important to understand is the quantum yield. We use below equation, since the fluorescence lifetime and fluorescence quantum yield are connected via below formula:

$$\frac{\tau}{\phi_f} = \frac{k_F + k_{IC} + k_{ISC}}{k_F \cdot (k_F + k_{IC} + k_{ISC})} = \frac{1}{k_F} \qquad \text{Eq. 5}$$

By this equation we can calculate the quantum yield ϕ_f .We use reference samples associated with the measured fluorescence lifetime, assuming dynamic quencher, we can determine the quantum yield of the unknown sample as:

$$\frac{\langle \tau \rangle_{x,sample}}{\phi_{f,sample}} = \frac{\langle \tau \rangle_{x,reference}}{\phi_{f,reference}} \qquad \text{Eq. 6}$$

There are different methods for measuring the lifetime, such as time correlated single photon counting (TCSPC) where the sample is excited by a pulse source (Novo, Felekyan, Seidel, & Al-Soufi, 2007).

Furthermore, due to the dispersion of the laser beam and electrical noise that can affect laser triggering, the instrument response function (IRF) needs to be removed from the

measured signal ($F_{(t)}$). Therefore, to obtain the multi exponential fluorescence decay a deconvolution approach is used (Lakowicz, 1999):

$$F(t) = IRF \otimes f(t) + IRF \qquad \text{Eq. 7}$$

The fluorescence decay and the deconvolution approach is shown Rhodamine 110 (descried below) is represented (Figure 2.2). The data was fit with a mono expansion model and the χ^2 shows the difference between fit and measurement data.

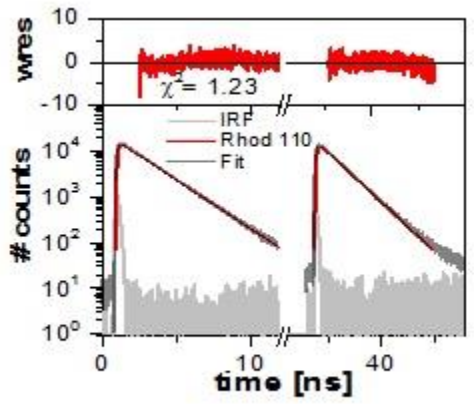

Figure 2.2 TCSPC plot for Rhodamine 110. The data (red) is connected from two color measurements that we have pulse laser for donor and acceptor and then it is fitted with mono expansion fit (black) and IRF (gray).

2.3) Quantum yield

As previously mentioned, electrons can be can be excited to the excited state by absorbing photons and then they can decay through non-radiative emission, fluorescence and other processes. Therefore, the emitted photons via fluorescence have lower energy compared to absorbed photons that is known as a stocks shift. So, the quantum yield (Φ_F) is the ratio of the emitted fluorescence photons by absorption photon, that is usually less than 1, although in rare situations it can be equal to 1:

$$\Phi_F = \frac{\#\text{ of emitted fluorescence photons}}{\#\text{ of absorbed photons}} = \frac{k_F}{k_F + k_{IC} + k_{ISC}} \leq 1 \qquad \text{Eq. 8}$$

To determine the quantum yield of an unknown sample, we assumed that only dynamic quenching takes place and that $\Phi_{FD}(0)$, Φ_{FA} are proportional to the species-averaged fluorescence lifetime $\langle\tau_{D(A)}\rangle$ of donor or acceptor, respectively. As reference samples we used Alexa488-labeled DNA $\langle D(0)\rangle_x$=4.0 ns, $\Phi_{FD}(0)$ = 0.8 and for the acceptor we used Cy5-labeled DNA with $\langle\tau_{D(A)}\rangle_x$= 1.17 ns and Φ_{FA} = 0.32 (Woźniak, Schröder, Grubmüller, Seidel, & Oesterhelt, 2008).

2.4) Fluorescence Anisotropy

Proteins and biomolecules rotate as they move. Through the solvent. Each sample can have different dynamic and rotational motions. Using polarized light as a source for excitation, the sample can absorb the light parallel to the dipole moment of the samples, and since the emitted light is polarized in different direction, the emission can occur in the parallel and perpendicular orientation. To quantify this we used fluorescence anisotropy, which can be written as:

$$r = \frac{F_{\parallel} - g \cdot F_{\perp}}{F_{\parallel} + 2 \cdot g \cdot F_{\perp}} \qquad \text{Eq. 9}$$

Where $F_{\parallel}$ and $F_{\perp}$ are the emission intensities measured parallel (0°) and perpendicular (90°) to the incident beam (0°) and g is a device dependent factor which corrects for the instruments non-idealities, e. g. unequal detection efficiencies of differently polarized light. Also, in the absence of the depolarization and non-rotational fluorophores, the fundamental anisotropy can be obtained from equation 10:

$$r_0 = 0.4\frac{3\cos^2(\beta)-1}{5} \qquad \text{Eq. 10}$$

Where r_0 is the maximum value this fluorophore can have - from which the angle between excitation and emission dipole β can be obtained and it is known as fundamental anisotropy. This value is the highest among the anisotropy measurements for the given molecule and in normal situations where that molecule has rotational motion, the anisotropy will be decreased. Moreover, the anisotropy for the molecule that is freely diffusing is related to lifetime and rotational correlation time via the Perrin equation (Weber, 1952):

$$r = \frac{r_0}{1+\tau/\rho} \qquad \text{Eq. 11}$$

Where ρ is rotation correlation time that depends on the viscosity, temperature and volume of the rotation of molecule. r_0 is the maximum value that fluorophore can have, and τ is the fluorescence life time.

2.5) Förster Resonance Energy Transfer

Förster resonance energy transfer (FRET) can give information about the distance and conformational changes in biological system. It requires the use of two different fluorophores whose spectrum of the donor emission and the acceptor absorption spectrum overlap (Rudy & Iverson, 1997). Moreover, the energy transfer depends on distance between donor (D) and acceptor (A), and was first described by Theodor Förster in 1948 (figure 2.3A,B)(Förster 1948). FRET relies on long- range dipole -dipole interactions between the donor and acceptor molecules and generally occurs between singlet states

($S_{1,\,Donor}$ to $S_{0,\,Acceptor}$) (Mely & Duportail, 2012). The main prerequisite for FRET is the spectra overlap to each other's, and it is called the overlap integral *J*. tIt is also showed in Figure 2.3C.

$$J(\lambda) = \int_0^\infty F_D(\lambda)\varepsilon_A(\lambda)\lambda^4 d\lambda \quad \text{Eq. 12}$$

where $F_D(\lambda)$ is the area-normalized donor emission, λ is wavelength, $\varepsilon_A(\lambda)$ is the wavelength dependent extinction coefficient of the acceptor and λ is wavelength. We can calculate the rate of the energy transfer via:

$$k_{FRET} = \frac{1}{\tau_D}\left(\frac{{R_0}^6}{{R_{DA}}^6}\right) \quad \text{Eq. 13}$$

The lifetime depends on the rate of the donor in the absence of the acceptor τ_D, R_{DA} is the distance between donor and acceptor, and R_0 is Förster radius that is the distance between donor and acceptor where 50% of the energy is transfer from a donor to an acceptor in fluorophore. FRET Efficiency (*E*) is related to fluorescence lifetime ($\tau_{D(0)}$, τ_{DA}), intensities (F_D, F_A) or distance between the two fluorophores (R_{DA}) via equation 14:

$$E = 1 - \frac{\tau_{DA}}{\tau_{D(0)}} = \frac{F_A}{F_D + F_A} = \frac{{R_0}^6}{{R_0}^6 + {R_{DA}}^6} \quad \text{Eq. 14}$$

Multiparameter fluorescence detection (MFD) that give information about static and dynamic behavior (in order of µs-ms) of the samples and different populations or conformational changes. Then, by using the photon distribution analysis (PDA) the kinetic and dynamicity of the samples can be analyzed in more details. Moreover, time resolved fluorescence lifetime measurement (TCSPC) is useful to get information in nanosecond about fluorescence lifetime and sample heterogeneity (Stanislav Kalinin,

Valeri, Antonik, Felekyan, & Seidel, 2010). This concept is explained in more detail above.

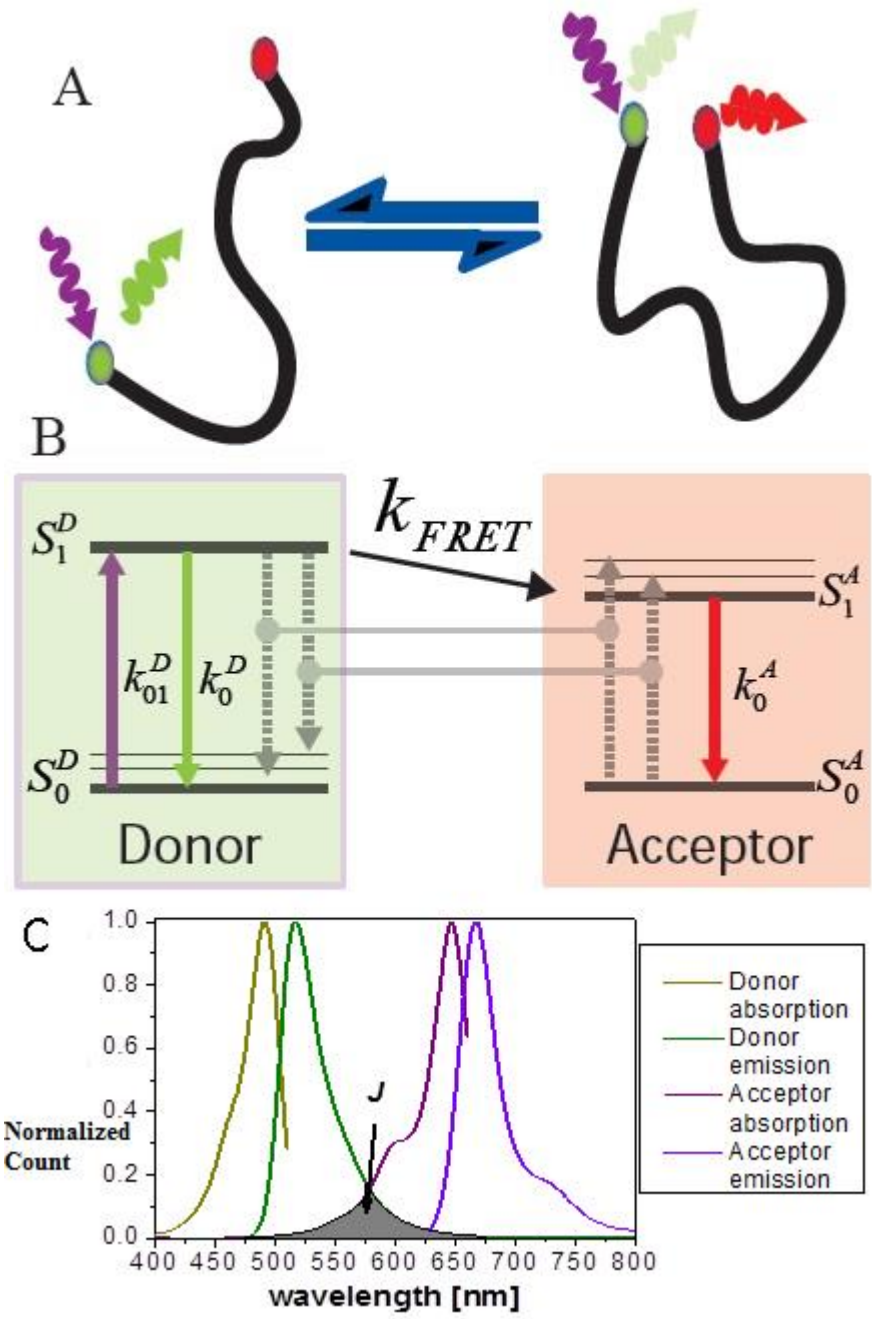

Figure 2.3Fluorescence Resonance Energy Transfer (FRET) to measure the inter dye distance in a dynamic molecule. A,B) Sketch of biomolecule labeling (donor (green) and acceptor (red), when the distance between donor and acceptor is long the absorption and emission of the donor is observed. However, when they are close, the energy from donor is

transferred to acceptor and the emission of the acceptor is observes. C) Overlap of spectrum of donor (Alexa 488) and acceptor (Alexa 647) (Modify picture from Sisamakis (2010)).

2.6) Multiparameter Fluorescence Detection (MFD)

MFD setup is a highly precise method to measure the single molecule fluorescence in a chamber on the confocal microscope in which a double labeled sample can freely move. By using a pulsed linearly polarized laser, the sample can be excited and the fluorescence emission is divided to four detectors, two for donor and two for acceptor (green and red). Each pair detect the parallel and perpendicular component. The signal from all four detectors are connected to time correlated single photon counting electronics, from which three parameters are determined for each photon event micro time (the time after each excitation pulse), macro time (the number of the pulse from starting before excitation of the sample) and detector number (Figure 2.4).

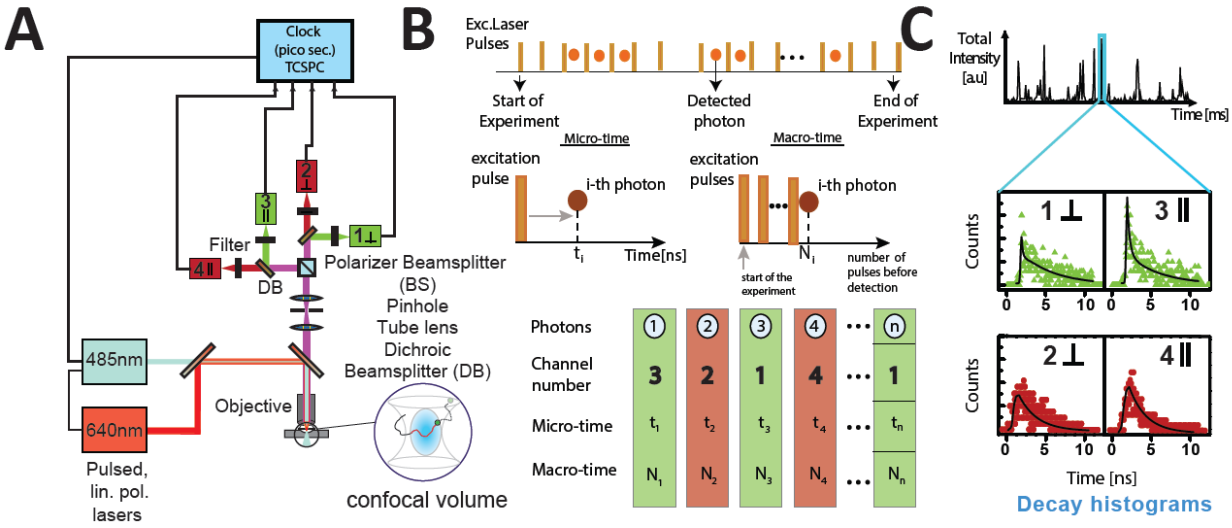

Figure 2.4Multiparameter Fluorescence Detection (MFD) set up and data collection. A) Confocal microscope set up and data collection. A) Confocal microscope set up used to measure single-molecule FRET experiments, and four detectors that is useful to measure tome correlated single photon counting. B) At least three parameters are determined by time correlated single photon counting (TCSPC) modules (Microtime, Macrotime, and channel number). C) The average fluorescence lifetime per single molecules enevt is obtained by fitting decay histograms of the recorded data (Modify from Clue's Seidel group)..

Single-molecule experiments performed in the course of this work are based on the so-called Burst-Integrated Fluorescence Lifetime (BIFL) method developed by Keller (Keller et al., 1996; Valeur & Brochon, 2001). This method was further advanced within the Seidel's group (Eggeling, Fries, Brand, Gunther, & Seidel, 1998; Kühnemuth & Seidel, 2001; Margittai et al., 2003; Rothwell et al., 2003) and the measurements were showed on a home-built four channel multiparameter fluorescence detection (MFD) setup (Qu, Chen, Zhou, Li, & Zhao, 2009)(Figure 2.4). With MFD is possible to build two dimensional histograms to gain information about the population distribution of the sample, the relationship between the ratio of the donor fluorescence over the acceptor fluorescence F_D/F_A over the fluorescence lifetime of donor. The relationship between the ratio of the donor fluorescence over the acceptor fluorescence F_D/F_A and the fluorescence weighted lifetime obtained in burst analysis $\langle \tau_{D(A)} \rangle$ depends on specific experimental parameters such as the fluorescence quantum yields of the dyes ($\Phi_{FD(0)}$ and Φ_{FA} for donor and acceptor respectively), background ($\langle B_G \rangle$ and $\langle B_R \rangle$ for green and red channels), detection efficiencies (g_G and g_R for green and red respectively) and crosstalk (α) . In the F_D/F_A vs. $\langle \tau_{D(A)} \rangle_f$ 2D representations it is useful to represent a static FRET line such as:

$$\left(\frac{F_D}{F_A}\right)_{\text{static}} = \frac{\Phi_{FD(0)}}{\Phi_{FA}} \cdot \left(\frac{\tau_{D(0)}}{\tau_{D(A)}} - 1\right)^{-1} \qquad \text{Eq. 15}$$

$\tau_{D(0)}$ is the donor fluorescence lifetime in the absence of acceptor. The corrected fluorescence (F_D and F_A) depends on other factors such as the detection efficiencies of green (g_G) and red (g_R) channels as follows:

$$F_D = \frac{S_G - \langle B_G \rangle}{g_G} \qquad \text{Eq. 16}$$

$$F_A = \frac{S_R - \alpha S_G - \langle B_R \rangle}{g_R} \qquad \text{Eq. 17}$$

where the total signal in red and green channels are S_R and S_G respectively. The ratio of fluorescence of donor divided by fluorescence of acceptor (F_D/F_A) is weighted by the species fractions. To properly describe the FRET line, it is important to consider that fluorophores are moving entities coupled to specific places via flexible linkers. This in turns generates a distance distribution between two fluorophores governed by the linker dynamics. Thus, the FRET line becomes:

$$\left(\frac{F_D}{F_A}\right)_{\text{static,L}} = \frac{\Phi_{FD(0)}}{\Phi_{FA}} \cdot \left(\frac{\tau_{D(0)}}{\langle \tau_{D(A)} \rangle_{\text{x,L}}} - 1 \right)^{-1} \qquad \text{Eq. 18}$$

For computing this, we need to consider the distance distribution between two fluorophores. We assume a Gaussian probability distance distribution with standard deviation σ_{DA} and mean value $\langle R_{DA} \rangle$ such as

$$p(R_{DA}) = \frac{1}{\sqrt{2\pi} \cdot \sigma_{DA}} \exp\left(\frac{-\left(R_{DA} - \langle R_{DA} \rangle\right)^2}{2\sigma_{DA}^2} \right) \qquad \text{Eq. 19}$$

For each R_{DA} one can calculate the corresponding species lifetime following

$$\tau_{D(A)}(R_{DA}) = \tau_{D(0)} \cdot \left(1 + \left(R_0 / R_{DA} \right)^6 \right)^{-1} \qquad \text{Eq. 20}$$

Where each species corresponds to different distances between the two fluorophores. For simplicity, the donor lifetime is treated as mono exponential decay ($\tau_{D(0)} = \langle \tau_{D(0)} \rangle_x =$

$\langle\tau_{D(0)}\rangle_f$.) Each $\tau_{D(A)}(R_{DA})$ has a probability defined by the corresponding distribution $p(t_{DA}(R_{DA}))=p(R_{DA})$. Therefore, the average species lifetime, due to linker dynamics, can be defined in the continuous approximation as

$$\left\langle \tau_{D(A)} \right\rangle_{x,L} = \int \tau_{D(A)}(R_{DA}) p(R_{DA}) dR_{DA} \qquad \text{Eq. 21}$$

and the fluorescence average lifetime as

$$\left\langle \tau_{D(A)} \right\rangle_{f,L} = \left\langle \tau_{D(A)} \right\rangle_{f} = \frac{\int \left(\tau_{D(A)}(R_{DA})\right)^2 p(R_{DA}) dR_{DA}}{\left\langle \tau_{D(A)} \right\rangle_{x,L}} \qquad \text{Eq. 22}$$

Thus, we can set a pair of parametric relations with respect to $\langle R_{DA}\rangle$ corresponding species to the species and fluorescence average lifetime such as

$$\left\langle \tau_{D(A)}(R_{DA}) \right\rangle_{x,L} \text{ and } \left\langle \tau_{D(A)}(R_{DA}) \right\rangle_{f,L} \quad \text{Eq. 23}$$

Therefore, by a numerical approximation we can create an empirical relation between the species and fluorescence average lifetimes for the selected range of $\langle R_{DA}\rangle$ using an first order polynomial function of with coefficients $A_{i,L}$ like

$$\left\langle \tau_{D(A)} \right\rangle_{x,L} = \sum_{i=0}^{n} A_i \left(\left\langle \tau_{D(A)} \right\rangle_{f,L} \right)^i \qquad \text{Eq. 24}$$

Finally, we introduce equation 25 to obtain the static FRET line corrected for dye linker movements

$$\left(\frac{F_D}{F_A} \right)_{\text{static,L}} = \frac{\Phi_{FD(0)}}{\Phi_{\text{FA}}} \cdot \left(\frac{\tau_{D(0)}}{\sum_{i=0}^{3} A_i \left(\left\langle \tau_{D(A)} \right\rangle_{f,L} \right)^i} - 1 \right)^{-1} \qquad \text{Eq. 25}$$

Coefficients (*A*'s) vary by experimental conditions, unless otherwise specified, we use in all figures and captions the assumption that all measured average lifetimes include the linker effect or $\langle t_{D(A)} \rangle_f = \langle t_{D(A)} \rangle_{f,L}$.

In the case of transition between two different states, one can also get an equation for a dynamic FRET line. In this case, a mixed fluorescence species arises from the interconversion between two conformational states. For the simplest case the dynamic FRET line can be analytically presented as (Sisamakis *et al.* 2010):

$$\left(\frac{F_D}{F_A}\right)_{dyn,L} = \frac{\Phi_{FD(0)}}{\Phi_{FA}} \cdot \frac{\langle \tau_1 \rangle_f \cdot \langle \tau_2 \rangle_f}{\tau_{D(0)} \cdot \left(\langle \tau_1 \rangle_f + \langle \tau_2 \rangle_f - \sum_{i=0}^{3} A'_i \left(\langle \tau_{D(A)} \rangle_{f,L} \right)^i \right) - \langle \tau_1 \rangle_f \cdot \langle \tau_2 \rangle_f} \quad \text{Eq. 26}$$

where $\langle t_{D(A)} \rangle_{f,L}$ is the mixed fluorescence lifetime and $\Phi_{FD(0)}$, Φ_{FA} are the quantum yields of the donor and acceptor dyes, respectively (S. Kalinin, S. Felekyan, A. Valeri, & C. A. Seidel, 2008a). $\langle t_1 \rangle_f$ and $\langle t_2 \rangle_f$ are two donor fluorescence lifetimes in presence of acceptor at the beginning and end points of the interconverting states. The $C_{i,L}$ coefficients are determined for each FRET pair and differ from the *A* coefficients. The *L* sub index notation is to identify and specify the linker effects.

In single molecule fluorescence experiments the number of detected fluorescence photons per burst is ~100. Therefore, a statistical efficient pattern needs to be applied to obtain fluorescence lifetime.

$$F(\tau, \rho, T) = \sum_{n=0}^{\infty} \left((IRF \otimes f(t))(t + n\omega) \right) \quad \text{Eq. 27}$$

where F is a realistic fluorescence pattern that is found by the convolution of the decay pattern function *f(t)* with an instrument response function *(IRF)* . However, it is limited

by frequency ω and arrival time window *t*. Also, the model patterns for the fluorescence decays in the parallel and perpendicular axis related to each polarization detector are

$$f_{\parallel}(\tau,\rho)=\frac{f(0)}{3}\exp(-t/\tau)[1+r(0)(2-3l_1)\exp(-t/\rho)] \qquad \text{Eq. 28}$$

$$f_{\perp}(\tau,\rho)=\frac{f(0)}{3}\exp(-t/\tau)[1+r(0)(1-3l_2)\exp(-t/\rho)] \qquad \text{Eq. 29}$$

l_1=0.0308 and l_2 =0.0368 that are the correction factor for changes due to the refraction index of the microscope objective lenses (Koshioka, Sasaki, & Masuhara, 1995; Schaffer et al., 1999), r_0 is the maximum value this fluorophore (equation 10).

In our experiment, we used Pulsed Interleaved Excitation (PIE) (Kudryavtsev et al., 2012) with two diode laser (Model LDH-D-C- 485 at 485 nm and laser LDH-D-C-640 at 640 nm; PicoQuant, Germany) operating at 40 MHz with 25 ns interleaved time. In this form it is possibleto alternate the excitation of the donor and the excitation of the acceptor. Therefore, other fluorescence properties pertaining mostly the acceptor fluorophore could be studied. The power at objective was set for 120 µW for the 485 nm laser line and 39 µW for the 640 nm excitation. Freely diffusing samples are excited as they pass through the confocal volume of a 60X, 1.2 NA collar (0.17) corrected Olympus objective. The emitted fluorescence signal was collected through the same objective and spatially filtered using a 70 µm pinhole, to define an effective confocal detection volume (Kong, Nir, Hamadani, & Weiss, 2007). The emitted fluorescence was divided into parallel and perpendicular components at two different colors (“green” and “red”) through band pass filters, ET525/50 and ET720/150, for green and red, respectively (Chroma Technology Co.) (Schaffer et al., 1999). In total four photon-detectors are used-

two for green (PMA Hybrid model 40 PicoQuant, Germany) and two for red channels (PMA Hybrid model 50, PicoQuant, Germany). A time correlated single photon counting (TCSPC) module (HydraHarp 400, PicoQuant, Germany) with Time-Tagged Time-Resolved (TTTR) mode and four synchronized input channels were used for data registration.

For smFRET measurement, donor-acceptor the labeled sample is diluted to pM concentration in buffer, which has been charcoal filtered to remove residual impurities. At pM concentration we assure that we observe 1 molecule per second. To prevent adsorption artifacts, NUNC chambers (Lab-Tek, Thermo Scientific, Germany) where pre-coated with a solution of 0.01% Tween 20 (Thermo Scientific) in water for 30 min and then rinsed included with ddH_2O. Collection time varied from several minutes up to 10 hours. Standard controls measuring water, to determine the instrument response function (IRF), buffer for background subtraction, and nM concentration of green and red standard dyes (Rhodamine 110, Rhodamine 101, and Alexa 647) in water for calibration of green and red channels, respectively. To calibrate the detection efficiencies we used a mixture solution of double labeled DNA oligonucleotides with known distance separation between donor and acceptor dyes.

Bursts are selected by 2σ criteria out of the mean background value with cut off times that vary from sample to sample with a minimum of 60 photons for each burst (Kühnemuth & Seidel, 2001; Schaffer et al., 1999). Each burst then is processed and fitted using a maximum likelihood algorithm (LabVIEW, National Instruments Co.,

Seidel's group) (Maus et al., 2001). Additional cut values for burst selections is needed based on each samples.

2.7) Photon Distribution analysis (PDA)

The fluorescence emission can be affacted by dye photophysics, dynamic motion of the sample, background count rate, spectral crosstalk and other factors that affect the signal of fluorescence as shot noise (all Poissonian distributed). FRET efficiency distribution is characterized by a Gaussian distribution with mean distance *R* and half-width hw_{DA}.

In MFD diagrams it is possible to get information about dynamics of the samples, but the accurate analysis and dynamic exchange is analyzed by an extension of the PDA theory, dynamic PDA *(dPDA)*. dPDA can fit experimental FRET efficiency distribution to obtain information about individual states and it can be used extract any additional broadening effects on FRET distributions (Antonik, Felekyan, Gaiduk, & Seidel, 2006; S. Kalinin, Felekyan, Antonik, & Seidel, 2007). The measured fluorescence signal *S*, consisting of fluorescence (*F*) and background (*B*) photons are expressed in photon count numbers per time window (Δt) of a fixed length. In Multiparameter Fluorescence Detection (MFD) the signal is split into two spectral windows termed "green" and "red" each with two polarization components (Parallel "||" and Perpendicular "⊥"). The probability of observing a certain combination of photon counts in two detection channels 1 and 2 (e.g., "1=green" and "2=red") and measured by two photon counting detectors. $P(S_1, S_2)$, is given by a product of independent probabilities

$$P(S_1, S_2) = \sum_{F_1+B_1=S_1; F_2+B_2=S_2} P(F)P(F_1, F_2 \mid F)P(B_1)P(B_2) \quad \text{Eq. 30}$$

$P(F)$ describes the fluorescence intensity distribution, i.e., the probability of observing exactly F fluorescence photons per time window (Δt). $P(B_1)$ and $P(B_2)$ represent the background intensity distributions. $P(F_1, F_2 \mid F)$ is the conditional probability of observing a particular combination of F_1 and F_2, provided the total number of fluorescence photons is F *(S. Kalinin et al., 2007)*. This can be expressed as

$$P(F_1, F_2 \mid F) = \frac{F!}{F_1! F_2!} p_1^{F_1} p_2^{F_2} = \frac{F!}{F_1!(F-F_1)!} p_1^{F_1} (1-p_1)^{F-F_1} \qquad \text{Eq. 31}$$

P_1 stands for the probability of a detected photon to be registered by the first detector (e.g., green in a FRET experiment or parallel in an anisotropy experiment). For the case of single molecule fluorescence experiments $p_1 = p_{\parallel}$ and consequently, $p_2 = p_{\perp}$. For smFRET p_1 is unambiguously related to the FRET efficiency E according to

$$p_1 = \left(1 + \alpha + \frac{E\Phi_{FA}}{(1-E)G\Phi_{FD(0)}} \right) \quad p_2 = 1 - p_1 \qquad \text{Eq. 32}$$

Here, G stands for the ratio of the detection efficiencies in the spectral windows ($G = g_G/g_R$) and the quantum yields ($\phi_{FD(0)}$ and ϕ_{FA}) were previously defined.

The distribution $P(F)$ in Eq. 25 is not directly measurable, instead the total signal intensity distribution $P(S)$ is measured, which is given by

$$P(S) = P(F) \otimes P(B) \qquad \text{Eq. 33}$$

where $P(B)$ is the distribution probability of background counts. Details on the deconvolution procedure are described elsewhere (S. Kalinin et al., 2007). Finally, this equation can be extended for multiple species with the brightness correction used in this work (S. Kalinin, S. Felekyan, A. Valeri, & C. A. M. Seidel, 2008b). Each species

distributions have a half width (hw_{DA}) which depends mostly in shot noise and photophysical properties of the acceptor fluorophore.

To model the shape of the F_D/F_A distributions we use probability distribution analysis or PDA (S. Kalinin et al., 2007)

Therefore, by using the various fitting model we can get information about the conformational changes and the rate of exchanges between states in different time windows in milliseconds time scales. Also, it is possible to analyze the data globally and obtain average information from all time windows.

2.8) Accessible Volume Simulation (AVSim)

The structure of the examined proteins can be determined by X-ray or NMR experiments or a computed homology models. In FRET measurement, we can use these techniques as a starting model and the distances can be estimated beforehand. Therefore, it is useful to determine optimal labeling positions such that, the distances between the donor and acceptor lie within the FRET-measurable range. Also, suspected motions and structure rearrangement of the biomolecules during reaction should lie in same measurement range.

Fluorophores that are used for labeling are attached to amino acid or nucleic acid site chains and contain additionally a flexible linker that serves as a spacer between the surface of the biomolecule and the fluorophore (Kasianowicz, 2002). Therefore, Instead of a single fixed measurable distance, thus, both dyes can explore a certain space volume only by its linker length and steric hindrance of the biomolecules ’surface.

To take this free movement of the dyes into account, an“ Accessible Volume Simulation ” (AVSim) can be performed (Muschielok *et al* .2008 ; Sindbert *et al* .2011) .Here, the dyes are modeled as sphere with three dye radius $R_{dye(i)}$ and the linker being a flexible cylinder of length L_{link} and width w_{Link} (Figure 2.5).

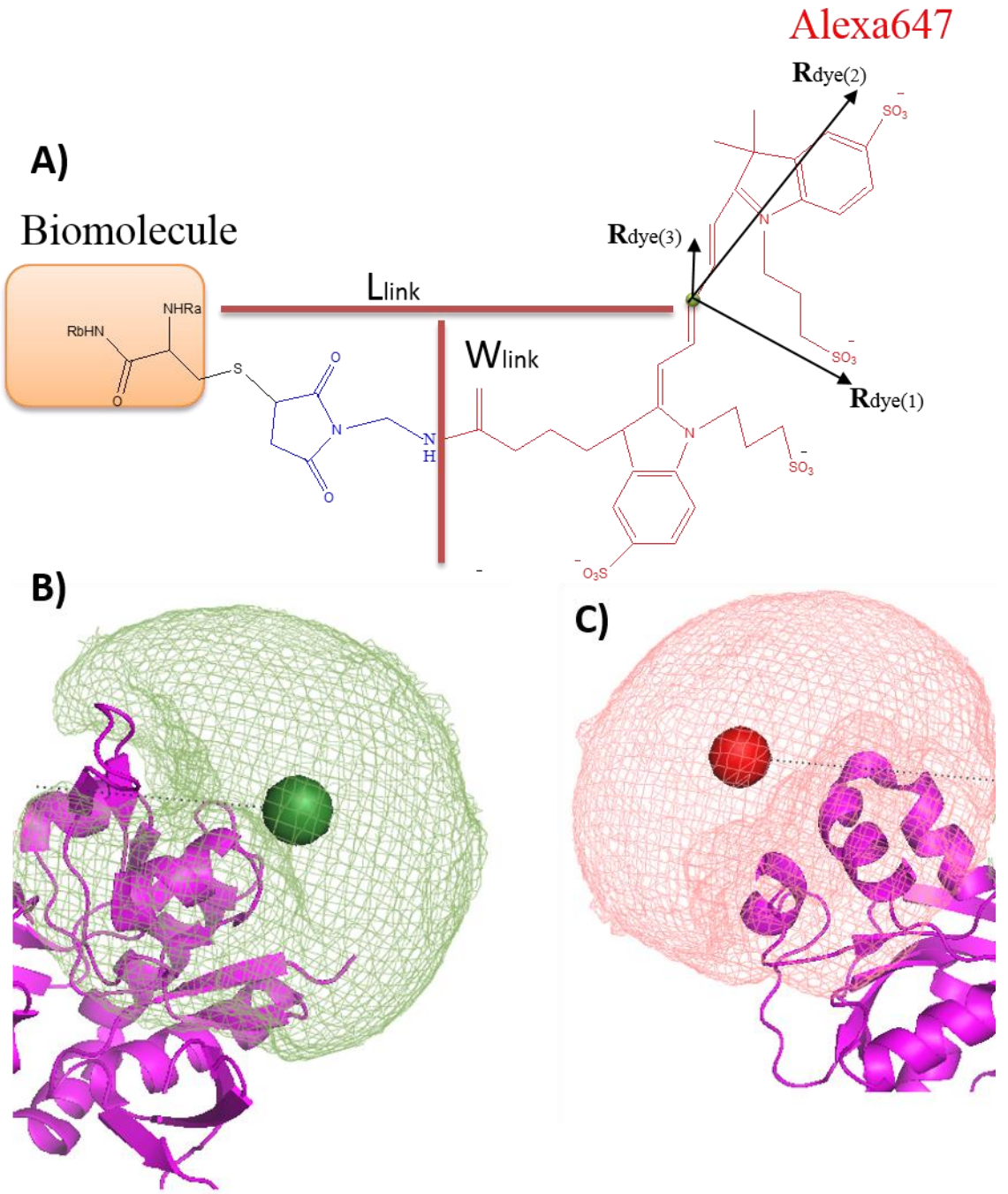

Figure 2.5 Schematic representation of a dye approximation with AVSim. A) Structure of Alexa 647 maleimide coupled to a biomolecule and the simplification used within AVSim Fluorephores are approximated by a sphere with a defined radius R_{dye} and the connection linker. B, C) Examples of AVSim for Alexa488-hydroxylamide and Alexa 647-maleimide for NMDA receptor. The dye accessible space volume is shown as mesh, the mean dye position as a sphere.

After identification of the label size and labeling sites, the program will first, attach the fluorophores to the provided structure, and in a second step, determine all possible configuration/position the dyes can take. Finally, from this set of possible positions the distances between the dyes can be calculated. Here, one has to differentiate between two different averaging distances

For each pair of AV's, we calculated the distance between dye mean positions (R_{mp})

$$R_{mp} = \left| \left\langle \vec{R}_{D(i)} \right\rangle - \left\langle \vec{R}_{A(j)} \right\rangle \right| = \left| \frac{1}{n} \sum_{i=1}^{n} \vec{R}_D^{(i)} - \frac{1}{m} \sum_{j=1}^{m} \vec{R}_A^{(j)} \right| \quad \text{Eq. 34}$$

where $\vec{R}_D^{(i)}$ and $\vec{R}_A^{(j)}$ are all the possible positions that the donor fluorophore and the acceptor fluorophore can take. However, in intensity based measurements, the mean donor-acceptor distance is determined by the integration time, thus the effective distance becomes:

$$\left\langle R_{DA} \right\rangle_E = R_0 \left(\left\langle E \right\rangle^{-1} - 1 \right)^{1/6} \text{ with}$$

$$\left\langle E \right\rangle = \frac{1}{nm} \sum_{i=1}^{n} \sum_{j=1}^{m} \left(\frac{R_0}{R_0 + \left| \overrightarrow{R_D^{(i)}} - \overrightarrow{R_A^{(j)}} \right|^6} \right) \quad \text{Eq. 35}$$

$\left\langle E \right\rangle$ is the average FRET efficiency. This distance, can also be modeled with the accessible volume calculation.

The relationship between R_{mp} and $\langle R_{DA} \rangle_E$ can be derived empirically following a third order polynomial from many different simulations.

The accessible volume considers the dyes as hard sphere models connected to the protein via flexible linkers (modeled as a flexible cylindrical pipe) (Klostermeier & Millar, 2002;

Sindbert et al., 2011). The overall dimension (width and length) of the linker is based on their chemical structures. For Alexa 488 the five carbon linker length was set to 20 Å, the width of the linker is 4.5 Å and the dye radius 3.5 Å. For Alexa 647 the dimensions used were: length = 22 Å, width = 4.5 Å and the dye radius = 3Å. Similar approaches have been introduced before to predict possible positions for EPR and FRET labels (Cai et al., 2007; S. P. Kalinin, T.; Sindbert, S.; Rothwell, P. J.; Berger, S.; Restle, T.; Goody, R. S.; Gohlke, H.; Seidel, C. A. M., 2012; Muschielok et al., 2008).

2.9) Purification of the protein

By using the standard side-directed mutagenesis protocol, it is possible to mutate the gene to encode Cysteines at this desired sites. Then, the plasmid is transformed to *Esherichia coli*, and cultures of transformed *E. coli* is grown until the culture reached an optical density of 0.8. At this point, protein expression was induced using 0.5 mM Isopropyl-1-thio-β-D-galactopyanoside, and expression is allowed to proceed at 20 ˚C for 24 hours. Cultures were then harvested, pelleted, and then stored at -80 ˚C until purification.

After thawing, induced *E. coli* pellets were further lysed using a cell disruption vessel (Parr instruments). Cell debris were pelleted at 185,000 g for 1 hour at 4 ˚C, and the GluN1 S1S2 in the supernatant was loaded onto an immobilized metal affinity chromatography column that had been previously charged with nickel sulfate (HiTrap HP, GE) using fast protein liquid chromatography (AKTA, GE). Purified GluN1 S1S2 was then eluted using a linear gradient of imidazole (Sigma).

2.10) FRET Labeling of the sample

The sulfate group of the introduced cysteines can be specifically labeled with preselected fluorophores optimal for FRET experiments (e.g. Alexa 488 as the donor and Alexa 647 as acceptor (Invitrogen)). Excess dye was removed by again purifying the protein onto a nickel affinity column (Ni-NTA agarose, Qiagen), and imidazole used for elution was removed using a PD-10 desalting column equilibrated with PBS (GE Lifesciences). Then, by using high UV-absorption the concentration and degree of labeling was determined.

CHAPTER THREE

NMDA RECEPTOR

3.1) Introduction

Ionotropic glutamate receptors (iGluRs) are a family of ligand-gated ion channels, which include the α-amino-3-hydroxy-5-methyl-4-isoxazolepropionic acid (AMPA) receptor, the kainate receptor, and the *N*-methyl-D-aspartate (NMDA) receptor (Traynelis et al., 2010). In the central nervous system, when an action potential stimulates the release of glutamate from an axon terminal, the glutamate diffuses across the synapse where it acts as a neurotransmitter by binding to the iGluRs. The binding of glutamate to the iGluRs occurs at the aptly named ligand-binding domain (LBD), an extracellular domain of the protein, which folds into a clamshell shape. The LBD, in the resting conformation, has an open cleft and the presence of glutamate or other agonists induces a closure of the clamshell cleft. This initial conformational change induces a series of other changes that open the channel. It follows that cations flow across the postsynaptic membrane, and the electrical signal propagates to the postsynaptic neuron (Bjerrum & Biggin, 2008).

Because of this pivotal role of the LBD to the iGluRs, numerous studies have been done to thoroughly examine the link between LBD conformation and iGluR function. Various studies into the AMPA receptor LBD have revealed a graded cleft closure mechanism—while full agonists such as glutamate that fully activate the channel also fully close the clamshell cleft; partial agonists, which only partially activate the channel, seem to stabilize a partially closed conformational intermediate (Gonzalez, Rambhadran, Du, & Jayaraman, 2008; Kudryavtsev et al., 2012; Kumar & Mayer, 2013; Maltsev, Ahmed,

Fenwick, Jane, & Oswald, 2008). Thus, activation of the AMPA receptor seems to be dictated by the extent to which an agonist can close its LBD cleft (Ahmed et al., 2013; Ramaswamy et al., 2012). Ensemble-based studies using a luminescence resonance energy transfer technique also seemed to show a similar mechanism with the glutamate-binding LBD of the NMDA receptor (Rambhadran, Gonzalez, & Jayaraman, 2011).

In comparison to other iGluRs, the NMDA receptor is unique, it has a very vital role in learning, memory, excitatory transmission in synapses, synaptic plasticity, and neuronal development. This receptor is named after the due to N-Methyl-D-Aspartate (NMDA) that can bind as an agonist molecule specifically just to the NMDA receptor.

There are some diseases that can affect NMDA receptor function and since this receptor is very important for brain function. For example, anti-NMDA receptor encephalitis it occurs when the immune system attack the NMDA receptor. The cause of this disease is unknown, but evidence show tumor grow in neural tissue.

The NMDA receptor is a hetero tetramer (about 97 kDa), that consists of two Glu1 and two Glu2 subunits. Each of the subunits has membrane-embedded helix, bilobed domain where the ligand can bind site, transmembrane helix, and bi-lobed amino terminal domain (Huggins & Grant, 2005). The three major parts are the amino-terminal domain (ATD) that helps the assembly of proteins, the transmembrane domain (TM) that has mostly hydrophobic amino acids to interact with membrane, and it is responsible for channel pore opening.

The last part is the ligand binding domain (LBD). This receptor is blocked by magnesium, but it is voltage dependent and when glutamate and other co-agonist bind to

ligand binding domain (LBD) the magnesium is removed and ions can pass through the receptor (Figure 3.1)(Byrne, Heidelberger, & Waxham, 2014). More significant, in addition glutamate, the NMDA receptor requires a co-agonist such as Glycine or D-serine for channel activation. This co-agonist similarly binds to a clamshell-shaped LBD on the GluN1 subunit, which shows cleft closure upon addition of the ligand. However, crystal studies of the GluN1 LB shows no difference in the extent of cleft closure with different partial agonists, leading to the **hypothesis of a two-state model, in which the closed, active state is stabilized to varying degrees, rather than the multi-state model of AMPA** which is opened at various degrees (Furukawa, Singh, Mancusso, & Gouaux, 2005; Inanobe, Furukawa, & Gouaux, 2005; Jespersen, Tajima, Fernandez-Cuervo, Garnier-Amblard, & Furukawa, 2014). Consistent with this, computational simulations using umbrella sampling methods have revealed that the apo GluN1 LBD conformational landscape shows two free energy minima, with one minimum corresponding to a closed clamshell and the other to an open clamshell(Dai & Zhou, 2015; Yao, Belcher, Berger, Mayer, & Lau, 2013). The addition of agonist stabilizes the closed-clamshell conformation, with partial agonists stabilizing the conformation to a lesser degree.

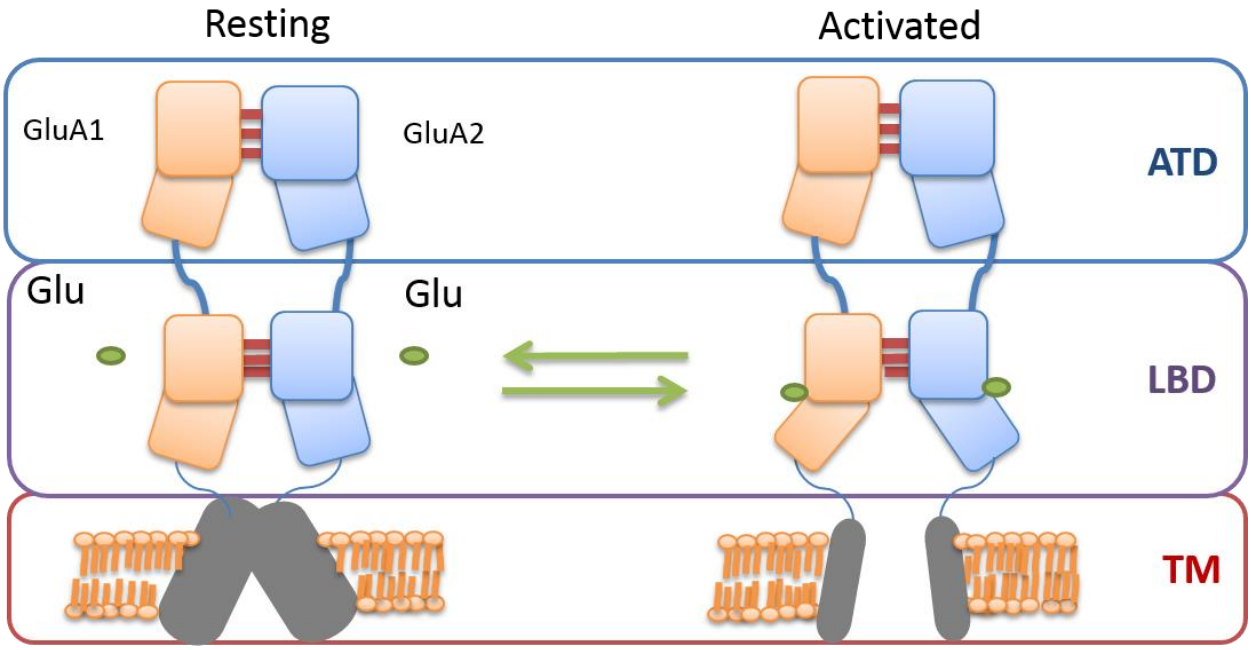

Figure 3.1 Sketch of NMDA receptor. When glutamate binds to the receptor then it has some conformational; changes and in the present of the co-agonist the ion channel becomes open (For simplicity just 2 of the subunits of this tetramer is shown)

Experimental verification of the two-state model has been attempted using fluorescence techniques. Early ensemble luminescence resonance energy transfer experiments did not show a difference in the cleft closure state among both full and partial agonists (Rambhadran et al., 2011), supporting the hypothesis of a single closed-cleft conformation; however, these studies were unable to resolve any difference in the stabilization of that closed state, which would be central to the mechanism of the two-state hypothesis (Kim, Kim, & Lee, 2015). More recently, single molecule Förster resonance energy transfer (smFRET) has been used in to experimentally observe the dynamic changes undergone by the GluN1 LBD (Cooper et al., 2015; Dolino et al., 2015). These studies provided the first experimental evidence of a partial agonist-dependent change in the conformational equilibrium of the GluN1 LBD; however, the time resolution for these experiments was limited to 10 ms. With the kinetic movements

of the GluN1 LBD occurring faster than this resolution (Kussius & Popescu, 2009) and the lack of a clear conformational model, more robust experimental methods were needed to clarify this mechanism of partial agonism.

In order to probe the conformational landscape of the GluN1 LBD at faster timescales than previously studied, we used multiparameter fluorescence detection (MFD) to obtain a complete experimental investigation of the receptor's dynamics and conformational equilibrium. MFD experiments can be used as another method of obtaining smFRET data, but in contrast to obtaining the intensity-based FRET efficiency of individual molecules over a period of seconds, MFD experiments measure a number of fluorescence parameters simultaneously, including intensity, lifetime, and anisotropy, of a population of molecules as they diffuse one at a time into a small confocal volume. The use of time-correlated single photon counting (TCSPC) allows for the exploration of dynamic motions in a broad range of timescales, down to picoseconds (S. Kalinin, Sisamakis, Magennis, Felekyan, & Seidel, 2010), making this method particularly well-suited for the task of experimentally observing the mechanism of partial agonism for the GluN1 LBD. As before (Cooper et al., 2015), the isolated GluN1 LBD was purified and site-directly labeled with fluorescent dyes to probe the distance across the LBD cleft (method section of chapter two it is described)(Figure 3.2). These results presented here have provided the first clear experimental evidence demonstrating a more complex mechanism than the up to date two-state model. We show that the GluN1 LBD exhibits a common closed-cleft, active arrangement among a variety of agonists, with partial agonists showing less stability of the closed conformation and more dynamic conversions to the open

conformations. We also reveal the existence of a third FRET state showing intermediate distance. This third FRET state may represent a sort of transition state of the protein wherein the two lobes of the LBD cleft have closed, but before subsequent ligand-conformational selection around the agonist have taken place (Figure 3.2).

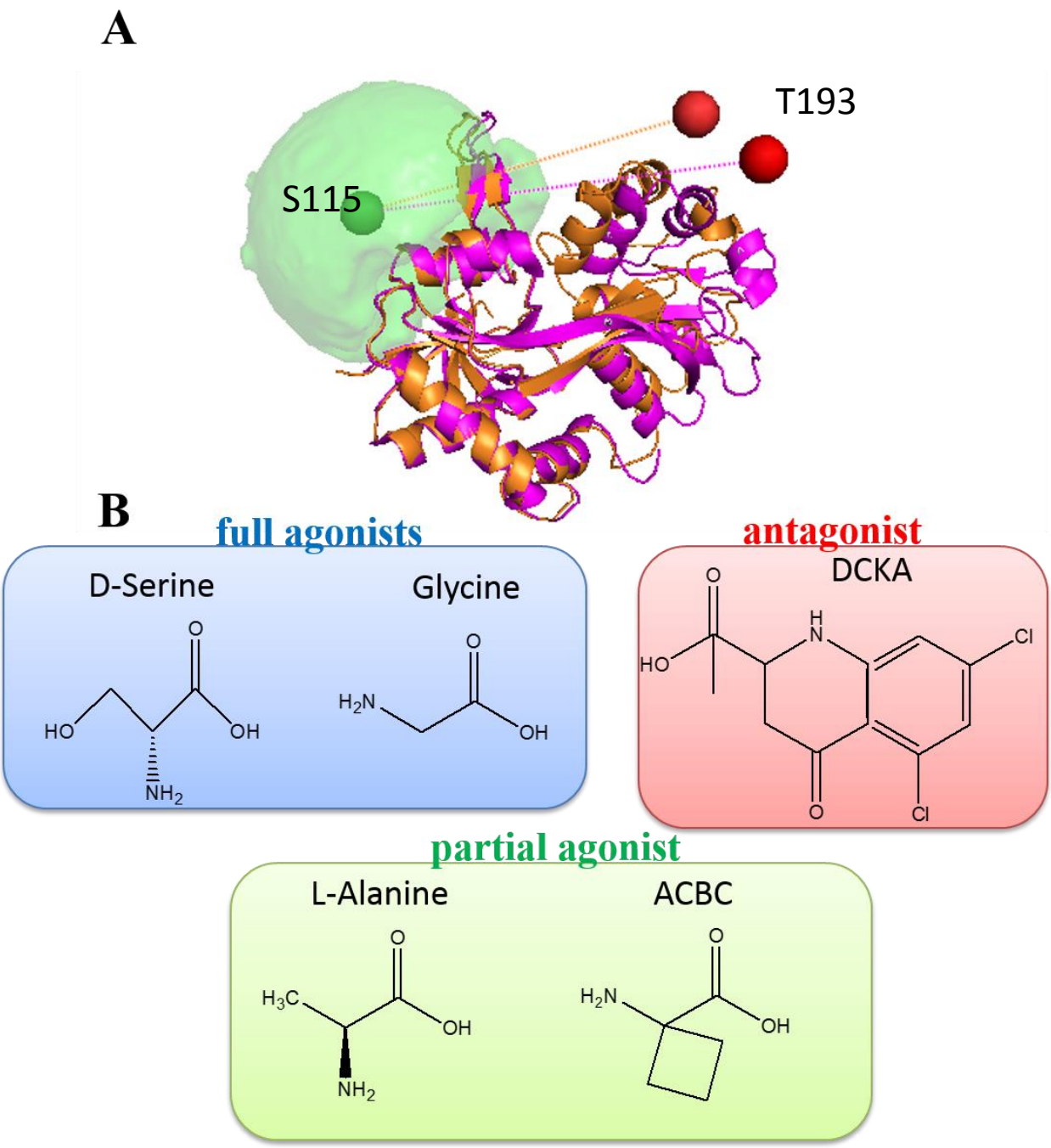

Figure 3.2 Cartoon representation of the NMDA receptor and ligands. A) The soluble domain NMDA recoptor(PDBID:1PB7,, pink). The accessible volume simulation calculate the available space that the fluorescent marker will occupy Green could represents the donor label (Alexa 488) at position S115 and the red cloud corresponds to the acceptor (Alexa 647) at T193. The interdye distance $\langle R_{DA} \rangle_{mp}$=44.8 A˚, $\langle R_{DA} \rangle_{E}$=48.7 A˚B) Structure of the ligands that are bind to LBD in NMDA receptor.

3.2) Results

The original construct for the *Rattus norvegicus* GluN1 S1S2 LBD in pET22b(+) was kindly donated by Eric Gouaux (Oregon Health Science Center, Portland, OR). The codons for Serine 115 and Threonine 193 of the construct, corresponding to Serine 507 and Threonine 701 of full-length GluN1 were mutated to encode Cysteine residues by using the method that described in chapter two. This plasmid was then transformed into Origami B (DE3) *Esherichia coli* (Novagen), and then cultures expressed, harvested and pelleted for purification, and also for this measurement, GluN1 containing cysteines at S115 and T193 was then labeled via method in chapter two.

To probe the GluN1 LBD dynamics, the isolated GluN1 LBD was labeled at Ser507 and Thr701 on opposite sides of the cleft(Cooper et al., 2015; Dolino et al., 2015)(Figure 3.2) using the FRET pair donor Alexa 488 and Alexa 647, which has an R_0 of 52 Å. Pulsed interleaved excitation (PIE) was used to excite the donor-acceptor (DA) labeled LBD samples in PBS buffer (50 mM sodium phosphate, pH 7.5, 150 mM NaCl), and emitted photons were collected to measure the FRET efficiency exhibited by single protein molecules when in complex with different ligands. FRET efficiency was measured simultaneously through both intensity measurements and donor lifetime measurements in a present of the acceptor. The resulting anisotropy and single-molecule events or burst histograms are presented in a multidimensional representation, where each event was preselected to remove those events with significant donor and acceptor photobleaching. In order to do that, fluorescent bursts were plotted in 2D histograms (Origin 8.6,

OriginLab Co), In addition, we used PIE to select those single-molecules with 1:1 donor to acceptor stoichiometry.

The results from anisotropy for different ligands are presented below (Figure 3.3). The red line shows the Perrine equation (equation 11 in chapter 2). As they indicate, for all the graphs the line pass through the mean bursts and we can obtain rotation of correlation time that is related to the size of the molecules (S. P. Kalinin, T.; Sindbert, S.; Rothwell, P. J.; Berger, S.; Restle, T.; Goody, R. S.; Gohlke, H.; Seidel, C. A. M., 2012).

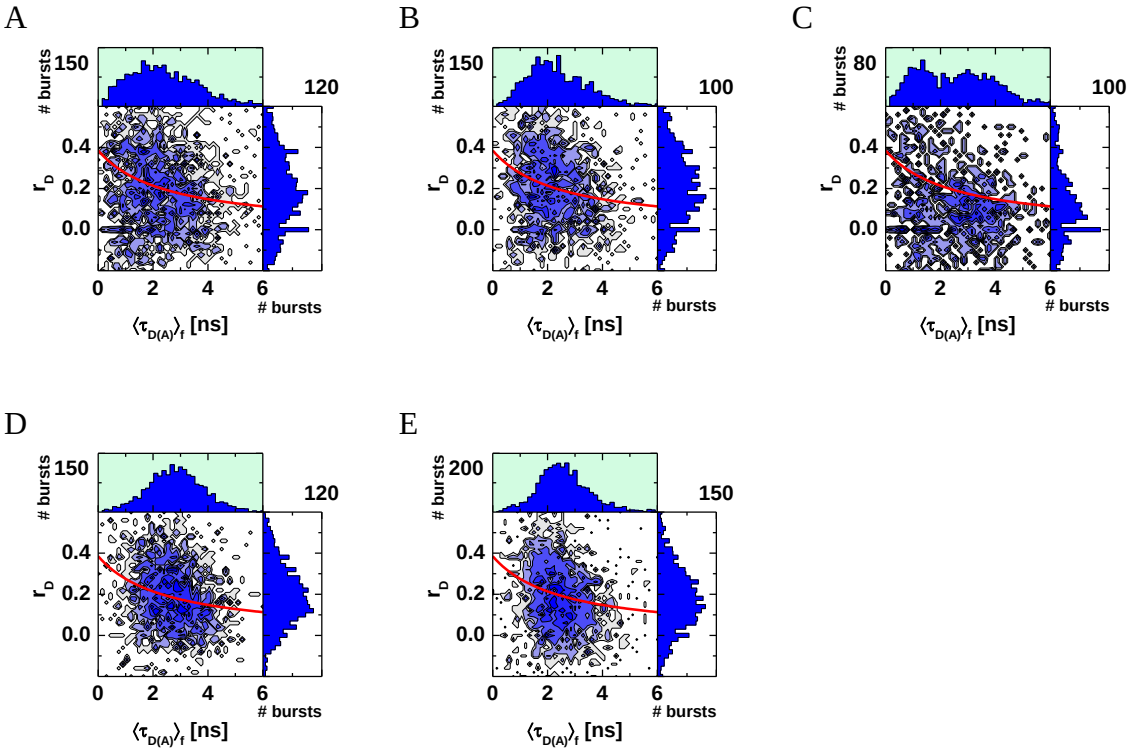

Figure 3.3 Anisotropy histograms. Two dimensional anisotropy histograms of LBD (Mutant) with multiple ligands and the red line described the relationship between anisotropy radius and the fluorescence averaged lifetime ($<\tau_{D(A)}>_f$)) .NMDA receptor with the present of various ligand. A) 1 mM GLY B) 1 mM D-Serine C) 15 mM Alanine D) 10 mM ACBC E) 0.1 mM DCKA.

The two dimensional MFD histograms based on average donor lifetime and ratio of donor-to-acceptor fluorescence can indicate the location of all FRET populations (S.

Kalinin et al., 2010). These histograms show clear differences in the conformational landscapes probed by the GluN1 LBD in complex with various ligands. As expected, with the antagonist 5,7-dichlorokynurenic acid (DCKA), mostly low-FRET states are explored with a longer donor fluorescence lifetime and a larger donor to acceptor fluorescence ratio (Figure 3.4E). This is consistent with the stabilization of an open-cleft conformation. When in complex to the full agonist glycine, FRET states shift toward higher efficiencies FRET, indicated by lower donor fluorescence lifetimes and smaller donor to acceptor fluorescence ratios (Figure 3.4A). This is also consistent with the stabilization of the closed-cleft conformation. A second full agonist, D-serine shows a similar trend (Figure 3.4B). In order to examine the LBD conformation and dynamics across a variety of activation states we examined two partial agonists (L-Alanine and 1-amino-1-cyclobutylcarboxylic acid or ACBC). Between the two, the more effective partial agonist L-alanine (Figure 3.3C) resembled more similarly the two full agonists, and the less effective partial agonist 1-amino-1-cyclobutylcarboxylic acid (ACBC, Figure 3.4D) resembled more similarly the antagonist FRET histogram. Of note, the histograms for the two partial agonists seemed to spread across a wider variety of conformational states. We identify that; these states must be to some extent static because they lie along the orange FRET line (Table 3.2). The orange sigmoidal line represents the static FRET line, which is the theoretical relationship between two FRET indicators: It is then evident that none of the ligands trap a single state of the LBD, but rather redistributes the population of the conformational states, consistent with conformational selection.

Table 3.1 donor and acceptor quantum yields

Sample	$F_{D(0)}$	F_{FA}
Gly	0.773	0.42
D-Serine	0.828	0.43
L-Alanine	0.843	0.41
ACBD	0.799	0.38
DCKA	0.850	0.40

Table 3.2 FRET Lines.Change tauf to the proper nomenclature.

Sample	Static FRET Line
Gly	(0.7732/0.4240)/((3.8660/((-0.0405*tauf^3)+(0.2914*tauf^2)+0.4891*tauf+-0.0422))-1)
D-Serine	(0.8286/0.4290)/((4.1430/((-0.0348*tauf^3)+(0.2676*tauf^2)+0.4977*tauf+-0.0443))-1)
L-Alanine	(0.8426/0.4130)/((4.2130/((-0.0335*tauf^3)+(0.2622*tauf^2)+0.4998*tauf+-0.0448))-1)
ACBD	(0.7990/0.3810)/((3.9950/((-0.0377*tauf^3)+(0.2799*tauf^2)+0.4932*tauf+-0.0432))-1)
DCKA	(0.8498/0.3960)/((4.2490/((-0.0329*tauf^3)+(0.2594*tauf^2)+0.5008*tauf+-0.0451))-1)
$<\tau D(A)>_f$	

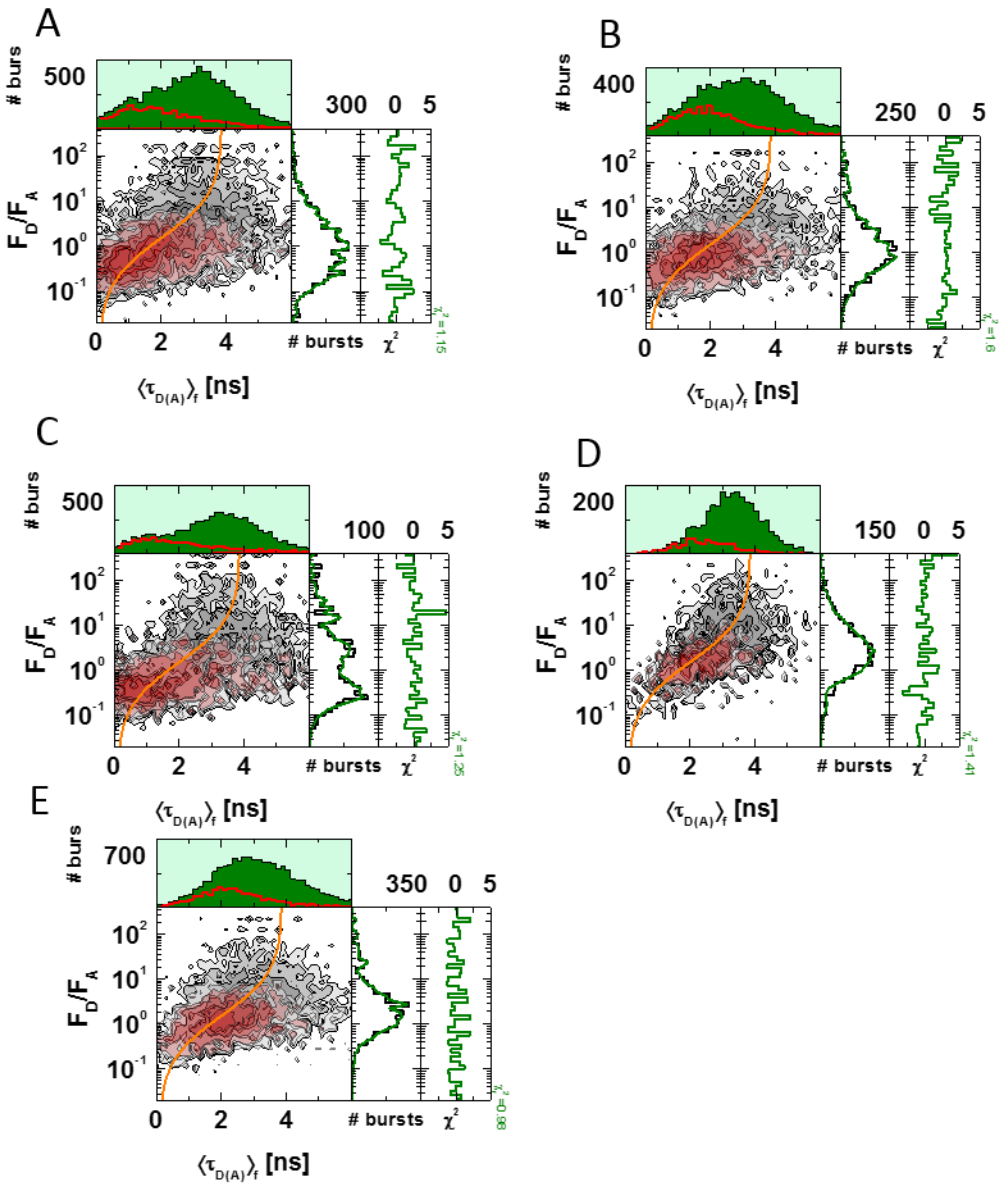

Figure 3.4 MFD histograms of LBD (Mutant) with multiple ligands. Two dimensional single molecule FRET histograms and one dimensional projections using TW=5 ms analysis PDA fit of FD/FA distribution of the same time window. The orange line described the relationship between FD/FA and the time-window fluorescence averaged lifetime (<$\tau_{D(A)}$>$_f$)) known as the static FRET line. NMDA receptor with the present of various ligand. A) 1 mM GLY B) 1 mM D-Serine C) 15 mM Alanine D) 10 mM ACBC E) 0.1 mM DCKA.

To improve the fit, we added the contribution of the donor-only population due to acceptor bleaching shows as red selection on Fig. 3.4 (red histograms on the 1D $\langle\tau_{D(A)}\rangle$ histogram projections). To fix that additional cuts are required that are include: first cut is

related to the difference in burst duration on green channels given donor excitation (T_{GX}) and burst duration on red channels given direct acceptor excitation (T_{RR}) was $-1.5<T_{GX}-T_{RR}<1.5$ (that is in the order of ms), whenever the signal from green channels are equal to the signal of the red channel then the difference is zero. However, sometimes donor and acceptor are quenched and we need to remove these events from the results of FRET measurement. Therefore, bursts also, needed to satisfy the FRET Stoichiometry (S_{PIE}) parameter of $0.1< S_{PIE} <0.6$ to select those bursts which have both fluorophores present and remove the donor and acceptor from FRET measurement. At the end, an additional selection based on the ratio of all uncorrected signal in the prompt channels (donor excitation TCSPC channels) over the overall collected photons across all collected TCSPC channels ($0.5<S_{prompt}/S_{Total}<0.8$) helped identify significant acceptor photobleaching during burst duration. This was clearly identified by the ratio of the prompt signal corresponding to the TCSPC channels of donor excitation (S_{prompt}) and total uncorrected signal of donor and acceptor emission (S_{prompt}/S_{Total}). S_{Total} is the signal over all TCSPC channels (Donor and acceptor excitation). The Stoichiometry parameter is corrected for quantum yield and detection efficiencies; however, the raw detected signal (S) does not require additional corrections. Therefore, this selection serves as an additional identification of events that smear towards the donor only population due to photobleaching. Moreover, we ruled out the possibility of a NO-FRET or very long interdye distance state because in the S_{prompt}/S_{Total} there were no leftover bursts with high enough F_D/F_A ratio with the same S_{prompt}/S_{Total} (Figure 3.5).

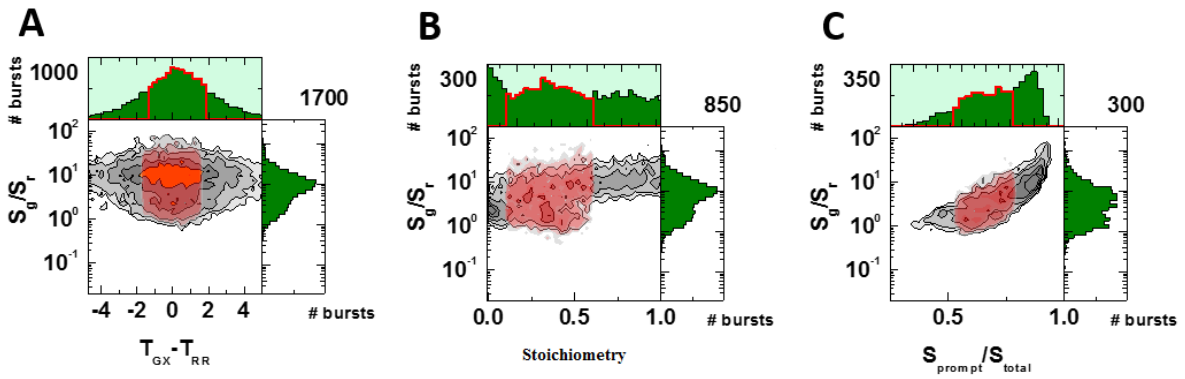

Figure 3.5 Diagram for burst selection. A) Difference between the signal of green channel (T_{GX}) and red channel (T_{RR}) due to acceptor bleaching (-1.5<T_{GX}-T_{RR}<1.5). B) Selecting the FRET samples, and removes donor and acceptor part. (0.1< S_{PIE} <0.6). C) Removing all acceptor photo bleaching, due to incorrect signal of promote channel over all data (0.5<S_{prompt}/S_{Total}<0.8).

In order to quantitatively analyze the conformational space and dynamic effects induced by ligand binding, we used probability distribution analysis (PDA) (S. Kalinin et al., 2007; S. Kalinin et al., 2008b; S. Kalinin et al., 2010). We used various models to fit the one-dimensional fluorescence ratio histograms with a time window of 5 milliseconds. When the time window selection is as close as possible to the burst duration, the analysis is similar to the steady state system. In our case, the burst duration is in the order of several milliseconds. Therefore, the selection of 5 ms is appropriate to reflect the overall integration time of each selected burst or single-molecule event. Moreover, we use PDA to identify the donor-acceptor distance $\langle R_{DA} \rangle$ distribution beyond shot-limit effects. To do so, we use Gaussian distributions that represent the interdye donor-acceptor distances for each FRET population. In PDA analysis, the width of each distribution is given by acceptor photophysics (Sisamakis, Valeri, Kalinin, Rothwell, & Seidel, 2010). In addition, PDA is used to identify dynamic processes in timescales similar to the chosen time window. To properly use PDA, it requires the use fitting models. Thus, to identify the model that best represents the experimental data, we carry a systematic approach of

identifying the minimum number of shot noise limit states. We reached a reasonable convergence with three different FRET states. In all conditions, the determined distances were very similar, and also the chi-square was around 1. Then, we fix all distances.

The next step after identifying the minimum number of FRET related conformations, we increased the level of complexity in the fitting model. For example, we know that intensity based FRET parameters are determined by fluctuations on the integrated acquisition time. PDA is particularly susceptible for capturing the blinking behavior of the dye generating by broaden the distribution beyond the shot limit case. This behavior has been well characterized (S. Kalinin et al., 2010). It is known that broadening is caused mostly due to acceptor blinking and it follows a monotonic relationship with respect to the interdye separation distance (S. Kalinin et al., 2010). Thus, each FRET related conformational states will have its own distribution of distances with a particular width (hw_{DA}) and mean interdye distance $\langle R_{DA}\rangle_E$. Note that R_{mp} and $\langle R_{DA}\rangle_E$ represent different "distances" (See accessible volume in the materials and methods section). Benchmark studies (S. P. Kalinin, T.; Sindbert, S.; Rothwell, P. J.; Berger, S.; Restle, T.; Goody, R. S.; Gohlke, H.; Seidel, C. A. M., 2012; Sindbert et al., 2011) have shown that 6% of the interdye distance $\langle R_{DA}\rangle_E$ is a typical effective width per state. Thus, we fixed the distribution width to 6%. To significantly improve the fitting or to reduce χ^2, we added a dynamic exchange between two FRET states (e.g. the χ^2 for glycan was 4.92 for tw=5 ms, but then by adding the dynamic exchange it reduced to 1.45 the same time window). Thus, the final fitting model consisted of 3 FRET conformational states, named HF, MF and LF plus one additional contribution of Donor Only, and a dynamics

equilibrium between the HF and MF. The addition of the dynamic state was only needed in the case of glycine, D-Serine and L-Alanine. For dynamic-PDA the same model needs to fit equally well various time windows. For example, if all states were static within the time-window, the static model would roughly fit all time windows equally well. This was the case of DCKA and ACBC. However, in the case of glycine, D-Serine and L-Alanine F_D/F_A distribution changed to a greater extent at multiple time windows (Δt = 5m, Δt = 2ms, and Δt = 0.5ms). Thus, there was a need of a dynamic process. For example, comparing glycine (full agonist) and L-Alanine (partial agonist) we identified that at short time windows Δt = 0.5ms, the F_D/F_A distribution, resembles significantly well the distribution found at Δt = 0.5ms (Fig. 3.6B and Fig 3.6A), even more so at an intermediate time window (Fig. 3.6B). However, this is not true for the partial agonist L-Alanine, where the distribution at Δt = 5 ms showed significant contribution at high FRET (Fig. 3.6D), but at shorter time windows (Fig. 3.6C-D) most of the population is found at the MF or LF states. This behavior is indicative of slower kinetics. Faster kinetics equilibrates the distribution at shorter time windows such as in the case of Glycine.

For this, we require to fit the model to the histograms obtained at various time windows. For example, if all states are static within the time-window, the static model would roughly fit all timewindow equally well. This was the case of DCKA and ACBC. However, in the case of Glycine, D-serine and L-Alanine F_D/F_A distribution changed to a greater extent at multiple time windows (Δt = 2ms, and Δt = 0.5ms) showed significant redistribution of the FRET indicator histograms (Figure 3.6).

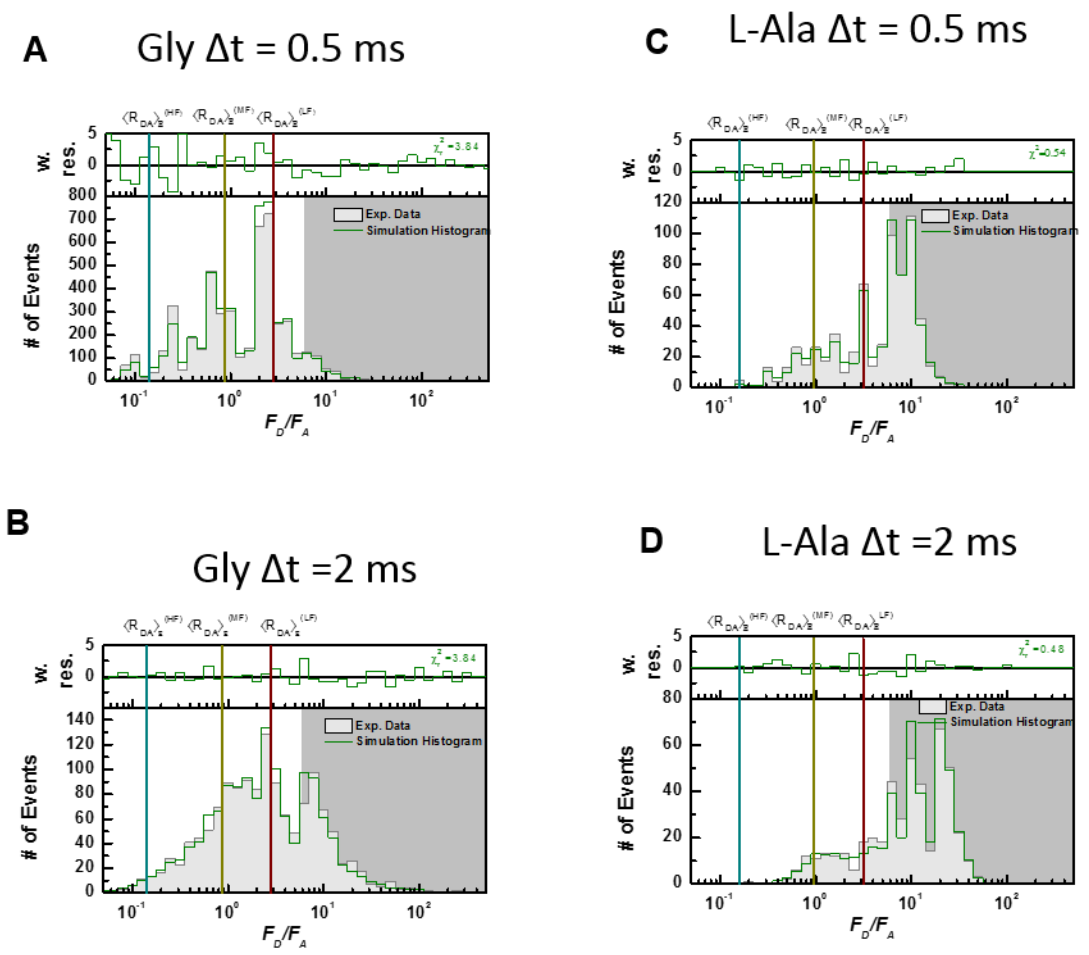

Figure 3.6 PDA comparison of LBD in the presence of Gly and L-Ala. Time window analysis for 0.5 and 2 (ms) for Gly and Alanine, A) and B) respectively. Same correction parameters are used as in Fig. 3.3 number of bursts vs. F_D/F_A indicates for NMDA ligand binding domain with Alanine has faster speed compared to GLY. PDA of static model fit for Alanine show that it does not fit well both time windows, although for Glycine it has lower speed and for both time windows it shows similar results.

For all ligands, we identified three FRET states with the following inter dye distances (Table 3.3): the High-FRET (HF) ($\langle R_{DA}\rangle_E$ = 33.9 Å), Medium-FRET (MF) ($\langle R_{DA}\rangle_E$ = 45.8 Å), and Low-FRET states (LF) ($\langle R_{DA}\rangle_E$ = 55.8 Å). Our results indicate that D-Serine excerpted the fastest exchange dynamics (t_R= 3.5 µs; Table 3.4), followed by glycine (t_R= 8 µs) and the slowest observed kinetics as expected by the time window analysis was L-Alanine with t_R= 50 µs.

Table 3.3 $\langle R_{DA} \rangle_E$ determined by PDA analysis

Sample	High-FRET (HF) [Å]	Medium-FRET (MF) [Å]	Low-FRET states (LF) [Å]
Gly	33.9	45.8	55.8
D-Ser	33.9	45.8	55.8
L-Ala	33.9	45.8	55.8
ACBD	33.9	45.8	55.8
DCKA	33.9	45.8	55.8

Table 3.4 Fastest relaxation time observed with PDA

Sample	t_R [ms]
Gly	0.0076
D-Ser	0.0035
L-Ala	0.05

Based on the results of PDA for multiple time windows, it is possible to split the contribution of states as those with fast dynamics and those seen as "static". It is then possible to identify the possible mechanistic activation of the LBD upon ligand-binding (Fig. 3.6). For example, in presence of DCKA the LBD al states appear "static". This means that there is no significant exchange dynamics between conformational states at the time scales of the burst duration (several milliseconds). At these timescales, three FRET states are required to describe the FRET indicator histograms; but the LBD is mostly found with the cleft open with the majority of the population in the LF and MF states (Fig. 3.7A). By adding ACBC, the NMDA cleft is also static, and it is found partially open (MF and LF) when compared to the DCKA. While ACBC is a partial

agonist it is so to a lesser extent than L-Alanine. Therefore, based on the results of PDA for multiple time windows, it is possible to split the contribution of the "static" states and those whose contribution arises from the dynamic contribution. It is then possible to identify the possible mechanistic activation of the LBD upon ligand binding (Fig. 3.7). For example, in presence of DCKA the LBD is "static", due to PDA results (χ^2 =1.72 for tw=5ms and when we added dynamic it changed to χ^2 =2.89). This means that there is no significant exchange dynamics between conformational states at the time scales of the burst duration (several milliseconds), and also in the present of DCKA the channel is closed and it moves slower but when the channel is open, then based on function it moves faster. At these timescales, three FRET states are required to describe the FRET indicator histograms; but the LBD is mostly found with the cleft open with the majority of the population in the LF state (Figure 3.7A). By adding ACBC, the NMDA cleft is also static, and it is found partially closed (HF and MF) when compared to the DCKA. We observe that the population of HF increases while the population of LF is decreased (Figure 3.7A). While ACBC is a partial agonist it is so to a lesser extent than L-Alanine.

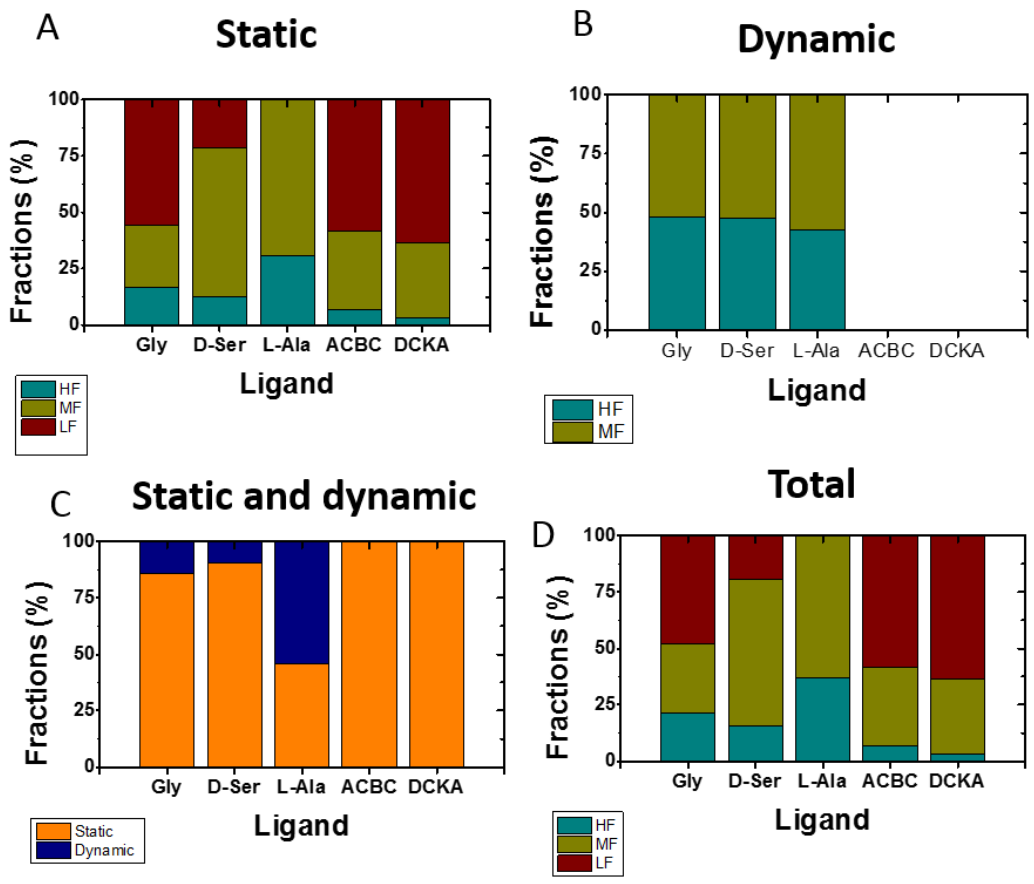

Figure 3.7 Fraction populations (static A, Dynamic B and static and dynamic C, total D) The High-FRET (HF)(<R_{DA}>$_E$= 33.9), Medium-FRET (MF)(<RDA>E= 45.8 A), and Low-FRET states (LF)(<R_{DA}>$_E$= 55.8 A) that respectively are shown by orange, purple and blue. Rate limiting stapes in the submillisecond/millisecond for various ligand with NMDA receptor from PDA analysis for time window 5 (ms). The results indicate DCKA and ACBC do not have any dynamic contributions. Although GLY that is agonist and Alanine and D-Serine that leads to partial agonist have dynamic behaviour. Alanine has more dynamic fraction compared to others.

Next, we compare L-Alanine to the full agonist Glycine. In both cases the closed configurations (LF and MF) as the majority. However, there is a clear difference to the contribution of the dynamic states (Fig. 3.7B-3.7C). While the dynamics fraction is higher for L-Alanine, it is also true that the relaxation time between the exchange between the HF and MF is slower (t_R= 50 μs; Table 3). For L-Alanine we find the dynamic is much faster with an effective exchange time of (t_R= 7.6 μs). D-serine has a

very similar effect as the full agonist Glycine. In this respect, the only major difference observed is the effective exchange time (t_R= 3.5 μs), which is faster than the Glycine. Overall, the combination of static and dynamic populations indicate that DCKA and ACBC are mostly static, while the other ligands have a dynamic contribution between the HF and MF states (Figure 3.7C-3.7D) and all the fraction including donor only is represented in Table 3.5.

Table 3.5 Overall fractions of PDA analysis including the donor-only (bleached fraction)

Sample	High-FRET (HF)	Medium-FRET (MF)	Low-FRET states (LF)	Donor only
Gly	59.35	14.48	5.52	20.65
D-Ser	9.75	37.05	11.1	42.6
L-Ala	13.59	11.5	0	63.6
ACBD	3.4	18	30.1	48.4
DCKA	2	21.5	40.8	18.3

3.3) Conclusion/Discussion

To clarify the mechanism of partial agonism, we have measured the cleft opening and closing motion of the LBD of the NMDA receptor in presence of the full agonists Glycine and D-Serine, partial agonist L-Alanine and ACBC (ordered by their effectiveness), and the full antagonist DCKA. The presence of the ligands redistributed the state populations, indicative of the conformational selection and preferred state. Even in the presence of ligands the LBD showed dynamic sampling of at least 3 different FRET conformations that could be separated with our FRET measurements. To quantify the dynamics, we used PDA and time window analysis to estimate the relative energy

landscape based on the population analysis presented in Fig. 3.6. The energy landscape in Fig. 3.7, shows that the full antagonists spends much of its time on the open cleft conformation leading to a closed channel. Although there is a significant fraction of MF, shared in all ligands, it seems that this conformation would not lead to activation of the channel. When comparing the measured FRET distance with the expected distances computed from the AV modeling using the crystallographic structure (PDBID: 1PB7) we obtain the experimentally determined MF distances is $\langle R_{DA} \rangle_E$ = 45.8 Å while the AV expected distance is $\langle R_{DA} \rangle_E$ = 48.7 Å. Thus, we can clearly see that the MF population resembles within 2.8 Å the crystallographic structure in presence of ligand.

Moreover, in Fig. 3.6 one could also observe that, although there are significant changes between various partial agonists and the full agonists. Faster kinetics is observed by the full agonists; and we found that the relaxation transition time of glycine differs by almost an order of magnitude on time compared to the dynamics observed in the partial agonist L-alanine. These findings are in agreement with single-channel recording of the opening and closing transitions, for which also a four state conformational transition was suggested (Kussius & Popescu, 2009). The authors suggested an intermediate, not fully active state that would lead to fully channel opening. This transition resembles the observed in our smFRET experiments. This two "closed" cleft configuration then seem to indicate the proper configuration for allosteric propagation resulting in channel opening.

REFERENCES

[1] Ahmed, A. H., Ptak, C. P., Fenwick, M. K., Hsieh, C. L., Weiland, G. A., & Oswald, R. E. (2013). Dynamics of cleft closure of the GluA2 ligand-binding domain in the presence of full and partial agonists revealed by hydrogen-deuterium exchange. *J Biol Chem, 288*(38), 27658-27666. doi:10.1074/jbc.M113.495564

[2] Alberts, B., Johnson, A., Lewis, J., Morgan, D., Raff, M., Roberts, K., & Walter, P. (2014). *Molecular Biology of the Cell*: Garland Science.

[3] Antonik, M., Felekyan, S., Gaiduk, A., & Seidel, C. A. (2006). Separating structural heterogeneities from stochastic variations in fluorescence resonance energy transfer distributions via photon distribution analysis. *Journal of Physical Chemistry B, 110*(13), 6970-6978. doi:10.1021/jp057257+

[4] Bax, A. (1989). Two-dimensional NMR and protein structure. *Annu Rev Biochem, 58*, 223-256. doi:10.1146/annurev.bi.58.070189.001255

[5] Bjerrum, E. J., & Biggin, P. C. (2008). Rigid body essential X-ray crystallography: distinguishing the bend and twist of glutamate receptor ligand binding domains. *Proteins, 72*(1), 434-446. doi:10.1002/prot.21941

[6] Brändén, C. I., & Tooze, J. (1999). *Introduction to Protein Structure*: Garland Pub.

[7] Bryngelson, J. D., Onuchic, J. N., Socci, N. D., & Wolynes, P. G. (1995). Funnels, pathways, and the energy landscape of protein folding: a synthesis. *Proteins, 21*(3), 167-195. doi:10.1002/prot.340210302

[8] Byrne, J. H., Heidelberger, R., & Waxham, M. N. (2014). *From Molecules to Networks: An Introduction to Cellular and Molecular Neuroscience*: Elsevier Science.

[9] Cai, Q., Kusnetzow, A. K., Hideg, K., Price, E. A., Haworth, I. S., & Qin, P. Z. (2007). Nanometer distance measurements in RNA using site-directed spin labeling. *Biophys J, 93*(6), 2110-2117. doi:S0006-3495(07)71465-0 [pii]10.1529/biophysj.107.109439

[10] Cavalli, A., Salvatella, X., Dobson, C. M., & Vendruscolo, M. (2007). Protein structure determination from NMR chemical shifts. *Proc Natl Acad Sci U S A, 104*(23), 9615-9620. doi:10.1073/pnas.0610313104

[11] Cooper, D. R., Dolino, D. M., Jaurich, H., Shuang, B., Ramaswamy, S., Nurik, C. E., . . . Landes, C. F. (2015). Conformational Transitions in the Glycine-Bound GluN1 NMDA Receptor LBD via Single-Molecule FRET. *Biophys J, 109*(1), 66-75. doi:10.1016/j.bpj.2015.05.025

[12] Crick, F. H., & Watson, J. D. (1956). Structure of small viruses. *Nature, 177*(4506), 473-475.

[13] Dai, J., & Zhou, H. X. (2015). Reduced curvature of ligand-binding domain free-energy surface underlies partial agonism at NMDA receptors. *Structure, 23*(1), 228-236. doi:10.1016/j.str.2014.11.012

[14] Deniz, A. A., Mukhopadhyay, S., & Lemke, E. A. (2008). Single-molecule biophysics: at the interface of biology, physics and chemistry. *Journal of the Royal Society Interface, 5*(18), 15-45. doi:10.1098/rsif.2007.1021

[15] Dolino, D. M., Cooper, D., Ramaswamy, S., Jaurich, H., Landes, C. F., & Jayaraman, V. (2015). Structural Dynamics of the Glycine-binding Domain of the N-Methyl-d-Aspartate Receptor. *Journal of Biological Chemistry, 290*(2), 797-804. doi:10.1074/jbc.M114.605436

[16] Eggeling, C., Fries, J. R., Brand, L., Gunther, R., & Seidel, C. A. (1998). Monitoring conformational dynamics of a single molecule by selective fluorescence spectroscopy. *Proc Natl Acad Sci U S A, 95*(4), 1556-1561.

[17] Engelborghs, Y., & Visser, A. J. W. G. (2013). *Fluorescence Spectroscopy and Microscopy: Methods and Protocols*: Humana Press.

[18] Fasman, G. D. (1996). *Circular dichroism and the conformational analysis of biomolecules*. New York: Plenum Press.

[19] Furukawa, H., Singh, S. K., Mancusso, R., & Gouaux, E. (2005). Subunit arrangement and function in NMDA receptors. *Nature, 438*(7065), 185-192. doi:10.1038/nature04089

[20] Gonzalez, J., Rambhadran, A., Du, M., & Jayaraman, V. (2008). LRET investigations of conformational changes in the ligand binding domain of a functional AMPA receptor. *Biochemistry, 47*(38), 10027-10032. doi:10.1021/bi800690b

[21] Greenfield, N. J. (2006). Using circular dichroism spectra to estimate protein secondary structure. *Nat Protoc, 1*(6), 2876-2890. doi:10.1038/nprot.2006.202

[22] Groves, M. J. (2005). *Pharmaceutical Biotechnology, Second Edition*: Taylor & Francis.

[23] Hartl, F. U., Bracher, A., & Hayer-Hartl, M. (2011). Molecular chaperones in protein folding and proteostasis. *Nature, 475*(7356), 324-332. doi:10.1038/nature10317

[24] Heilemann, M., Hwang, L. C., Lymperopoulos, K., & Kapanidis, A. N. (2009). Single-molecule FRET analysis of protein-DNA complexes. *Methods Mol Biol, 543*, 503-521. doi:10.1007/978-1-60327-015-1_29

[25] Huggins, D. J., & Grant, G. H. (2005). The function of the amino terminal domain in NMDA receptor modulation. *J Mol Graph Model, 23*(4), 381-388. doi:10.1016/j.jmgm.2004.11.006

[26] Inanobe, A., Furukawa, H., & Gouaux, E. (2005). Mechanism of partial agonist action at the NR1 subunit of NMDA receptors. *Neuron, 47*(1), 71-84. doi:10.1016/j.neuron.2005.05.022

[27] Jacobsen, N. E. (2007). *NMR Spectroscopy Explained: Simplified Theory, Applications and Examples for Organic Chemistry and Structural Biology*: Wiley.

[28] Jespersen, A., Tajima, N., Fernandez-Cuervo, G., Garnier-Amblard, Ethel C., & Furukawa, H. (2014). Structural Insights into Competitive Antagonism in NMDA Receptors. *Neuron, 81*(2), 366-378.

[29] Kalinin, S., Felekyan, S., Antonik, M., & Seidel, C. A. M. (2007). Probability distribution analysis of single-molecule fluorescence anisotropy and resonance energy transfer. *Journal of Physical Chemistry B, 111*(34), 10253-10262.

[30] Kalinin, S., Felekyan, S., Valeri, A., & Seidel, C. A. (2008a). Characterizing multiple molecular States in single-molecule multiparameter fluorescence detection by probability distribution analysis. *J Phys Chem B, 112*(28), 8361-8374. doi:10.1021/jp711942q

[31] Kalinin, S., Felekyan, S., Valeri, A., & Seidel, C. A. M. (2008b). Characterizing Multiple Molecular States in Single-Molecule Multiparameter Fluorescence Detection by Probability Distribution Analysis. *Journal of Physical Chemistry B, 112*(28), 8361-8374.

[32] Kalinin, S., Sisamakis, E., Magennis, S. W., Felekyan, S., & Seidel, C. A. M. (2010). On the origin of broadening of single-molecule FRET efficiency distributions beyond shot noise limits. *Journal of Physical Chemistry B, 114*, 6197–6206.

[33] Kalinin, S., Valeri, A., Antonik, M., Felekyan, S., & Seidel, C. A. M. (2010). Detection of structural dynamics by FRET: a photon distribution and fluorescence lifetime analysis of systems with multiple states. *J Phys Chem B, 114*(23), 7983-7995. doi:10.1021/jp102156t

[34] Kalinin, S. P., T.; Sindbert, S.; Rothwell, P. J.; Berger, S.; Restle, T.; Goody, R. S.; Gohlke, H.; Seidel, C. A. M. (2012). A toolkit and benchmark study for FRET-restrained high-precision structural modeling. *Nature Methods, 9*, 1218-1225.

[35] Kasianowicz, J. J. (2002). Nanometer-scale pores: potential applications for analyte detection and DNA characterization. *Dis Markers, 18*(4), 185-191.

[36] Keller, R. A., Ambrose, W. P., Goodwin, P. M., Jett, J. H., Martin, J. C., & Wu, M. (1996). Single molecule fluorescence analysis in solution. *Applied Spectroscopy, 50*(7), A12-A32. Retrieved from <Go to ISI>://WOS:A1996UZ54800002

[37] Kim, J. Y., Kim, C., & Lee, N. K. (2015). Real-time submillisecond single-molecule FRET dynamics of freely diffusing molecules with liposome tethering. *Nat Commun, 6*, 6992. doi:10.1038/ncomms7992

[38] Klostermeier, D., & Millar, D. P. (2002). Energetics of hydrogen bond networks in RNA: hydrogen bonds surrounding G+1 and U42 are the major determinants for the tertiary structure stability of the hairpin ribozyme. *Biochemistry, 41*(48), 14095-14102.

[39] Kong, X., Nir, E., Hamadani, K., & Weiss, S. (2007). Photobleaching pathways in single-molecule FRET experiments. *J Am Chem Soc, 129*(15), 4643-4654. doi:10.1021/ja068002s

[40] Koshioka, M., Sasaki, K., & Masuhara, H. (1995). Time-Dependent Fluorescence Depolarization Analysis in 3-Dimensional Microspectroscopy. *Applied Spectroscopy, 49*(2), 224-228. doi:Doi 10.1366/0003702953963652

[41] Kudryavtsev, V., Sikor, M., Kalinin, S., Mokranjac, D., Seidel, C. A. M., & Lamb, D. C. (2012). Combining MFD and PIE for Accurate Single-Pair Förster

Resonance Energy Transfer Measurements. *ChemPhysChem, 13*(4), 1060-1078. doi:10.1002/cphc.201100822
[42] Kühnemuth, R., & Seidel, C. A. M. (2001). Principles of single molecule multiparameter fluorescence spectroscopy. *Single Molecules, 2*(4), 251-254. Retrieved from <Go to ISI>://000174074800005
[43] Kumar, J., & Mayer, M. L. (2013). Functional Insights from Glutamate Receptor Ion Channel Structures*. *Annual Review of Physiology, 75*(1), 313-337. doi:doi:10.1146/annurev-physiol-030212-183711
[44] Kussius, C. L., & Popescu, G. K. (2009). Kinetic basis of partial agonism at NMDA receptors. *Nat Neurosci, 12*(9), 1114-1120. doi:10.1038/nn.2361
[45] Lakowicz, J. R. (1999). *Principles of Fluorescence Spectroscopy*: Kluwer Academic/Plenum.
[46] Maltsev, A. S., Ahmed, A. H., Fenwick, M. K., Jane, D. E., & Oswald, R. E. (2008). Mechanism of partial agonism at the GluR2 AMPA receptor: Measurements of lobe orientation in solution. *Biochemistry, 47*(40), 10600-10610. doi:10.1021/bi800843c
[47] Margittai, M., Widengren, J., Schweinberger, E., Schroder, G. F., Felekyan, S., Haustein, E., . . . Seidel, C. A. (2003). Single-molecule fluorescence resonance energy transfer reveals a dynamic equilibrium between closed and open conformations of syntaxin 1. *Proc Natl Acad Sci U S A, 100*(26), 15516-15521. doi:10.1073/pnas.2331232100
[48] Maus, M., Cotlet, M., Hofkens, J., Gensch, T., De Schryver, F. C., Schaffer, J., & Seidel, C. A. (2001). An experimental comparison of the maximum likelihood estimation and nonlinear least-squares fluorescence lifetime analysis of single molecules. *Anal Chem, 73*(9), 2078-2086.
[49] Mely, Y., & Duportail, G. (2012). *Fluorescent Methods to Study Biological Membranes*: Springer Berlin Heidelberg.
[50] Muschielok, A., Andrecka, J., Jawhari, A., Bruckner, F., Cramer, P., & Michaelis, J. (2008). A nano-positioning system for macromolecular structural analysis. *Nat Methods, 5*(11), 965-971. doi:nmeth.1259 [pii]
[51] 10.1038/nmeth.1259
[52] Nelson, D. L., Lehninger, A. L., & Cox, M. M. (2008). *Lehninger Principles of Biochemistry*: W. H. Freeman.
[53] Novo, M., Felekyan, S., Seidel, C. A. M., & Al-Soufi, W. (2007). Dye-exchange dynamics in micellar solutions studied by fluorescence correlation spectroscopy. *Journal of Physical Chemistry B, 111*(14), 3614-3624. doi:10.1021/jp0657639
[54] Olofsson, L., & Margeat, E. (2013). Pulsed interleaved excitation fluorescence spectroscopy with a supercontinuum source. *Opt Express, 21*(3), 3370-3378. doi:10.1364/OE.21.003370
[55] Phillips, R., Kondev, J., Theriot, J., & Garcia, H. (2012). *Physical Biology of the Cell, Second Edition*: Taylor & Francis Group.
[56] Powell, H. R. (1999). The Rossmann Fourier autoindexing algorithm in MOSFLM. *Acta Crystallogr D Biol Crystallogr, 55*(Pt 10), 1690-1695.

[57] Qu, P., Chen, X. D., Zhou, X. X., Li, X., & Zhao, X. S. (2009). Fluorescence quenching of TMR by guanosine in oligonucleotides. *Science in China Series B-Chemistry, 52*(10), 1653-1659. doi:10.1007/s11426-009-0235-4

[58] Ramaswamy, S., Cooper, D., Poddar, N., MacLean, D. M., Rambhadran, A., Taylor, J. N., . . . Jayaraman, V. (2012). Role of conformational dynamics in alpha-amino-3-hydroxy-5-methylisoxazole-4-propionic acid (AMPA) receptor partial agonism. *J Biol Chem, 287*(52), 43557-43564. doi:10.1074/jbc.M112.371815

[59] Rambhadran, A., Gonzalez, J., & Jayaraman, V. (2011). Conformational changes at the agonist binding domain of the N-methyl-D-aspartic acid receptor. *J Biol Chem, 286*(19), 16953-16957. doi:10.1074/jbc.M111.224576

[60] Richardson, J. S. (1981). The anatomy and taxonomy of protein structure. *Adv Protein Chem, 34*, 167-339.

[61] Rothwell, P. J., Berger, S., Kensch, O., Felekyan, S., Antonik, M., Wohrl, B. M., . . . Seidel, C. A. (2003). Multiparameter single-molecule fluorescence spectroscopy reveals heterogeneity of HIV-1 reverse transcriptase:primer/template complexes. *Proc Natl Acad Sci U S A, 100*(4), 1655-1660. doi:10.1073/pnas.0434003100

[62] Rudy, B., & Iverson, L. E. (1997). *Ion Channels*: Academic Press.

[63] Schaffer, J., Volkmer, A., Eggeling, C., Subramaniam, V., Striker, G., & Seidel, C. A. M. (1999). Identification of single molecules in aqueous solution by time-resolved fluorescence anisotropy. *Journal of Physical Chemistry A, 103*(3), 331-336. Retrieved from <Go to ISI>://000079042400001

[64] Sindbert, S., Kalinin, S., Hien, N., Kienzler, A., Clima, L., Bannwarth, W., . . . Seidel, C. A. M. (2011). Accurate Distance Determination of Nucleic Acids via Forster Resonance Energy Transfer: Implications of Dye Linker Length and Rigidity. *Journal of the American Chemical Society, 133*(8), 2463-2480. doi:10.1021/ja105725e

[65] Sisamakis, E., Valeri, A., Kalinin, S., Rothwell, P. J., & Seidel, C. A. M. (2010). Accurate single-molecule FRET studies using multiparameter fluorescence detection. *Methods in Enzymology, 475*, 456-514.

[66] Skoog, D. A., & Leary, J. J. (1992). *Principles of instrumental analysis*: Saunders College Pub.

[67] Smyth, M. S., & Martin, J. H. (2000). x ray crystallography. *Mol Pathol, 53*(1), 8-14.

[68] Sun, Y., Rombola, C., Jyothikumar, V., & Periasamy, A. (2013). Forster resonance energy transfer microscopy and spectroscopy for localizing protein-protein interactions in living cells. *Cytometry A, 83*(9), 780-793. doi:10.1002/cyto.a.22321

[69] Traynelis, S. F., Wollmuth, L. P., McBain, C. J., Menniti, F. S., Vance, K. M., Ogden, K. K., . . . Dingledine, R. (2010). Glutamate Receptor Ion Channels: Structure, Regulation, and Function. *Pharmacological Reviews, 62*(3), 405-496. doi:10.1124/pr.109.002451

[70] Valeur, B., & Brochon, J. C. (2001). *New Trends in Fluorescence Spectroscopy: Applications to Chemical and Life Sciences : With 187 Figures and 39 Tables*: Springer.
[71] Varadi, M., Vranken, W., Guharoy, M., & Tompa, P. (2015). Computational approaches for inferring the functions of intrinsically disordered proteins. *Front Mol Biosci, 2*, 45. doi:10.3389/fmolb.2015.00045
[72] Weber, G. (1952). Polarization of the fluorescence of macromolecules. II. Fluorescent conjugates of ovalbumin and bovine serum albumin. *Biochem J, 51*(2), 155-167.
[73] Woźniak, A. K., Schröder, G., Grubmüller, H., Seidel, C. A. M., & Oesterhelt, F. (2008). Single molecule FRET measures bends and kinks in DNA. *Proc.Natl.Acad.Sci.USA., 105*, 18337-18342.
[74] Yao, Y., Belcher, J., Berger, A. J., Mayer, M. L., & Lau, A. Y. (2013). Conformational analysis of NMDA receptor GluN1, GluN2, and GluN3 ligand-binding domains reveals subtype-specific characteristics. *Structure, 21*(10), 1788-1799. doi:10.1016/j.str.2013.07.011
[75] Zwanzig, R., Szabo, A., & Bagchi, B. (1992). Levinthal's paradox. *Proc Natl Acad Sci U S A, 89*(1), 20-22.